Diurnal cycles of cloud and rainfall over North–East Queensland during the coral bleaching season

Alanah Chapman[1,2,3,4], Yi Huang[1,2], and Claire Vincent[1,2]

[1]School of Geography, Earth and Atmospheric Sciences, The University of Melbourne
[2]ARC Centre of Excellence for 21st Century Weather, Melbourne, VIC, Australia
[3]CSIRO Environment, Melbourne, Australia
[4]Australian Antarctic Program Partnership, Institute for Marine and Antarctic Studies, University of Tasmania, Hobart, AU, Australia

Correspondence: Yi Huang (yi.huang4@unimelb.edu.au)

Abstract. Mass coral bleaching events are becoming increasingly frequent over the Great Barrier Reef (GBR), posing a critical risk to Australia's marine ecosystems and the broader global ocean environment. These events are primarily driven by anomalously warm water temperatures, but their severity is strongly influenced by local cloud cover, which controls the amount of solar radiation reaching the ocean surface (including ultra–violet radiation which exacerbates bleaching). This study presents a characterization of the cloud and rainfall diurnal cycles over north–east Queensland during the coral bleaching season, providing a foundational step to untangling the complex relationships between clouds, rainfall, local–scale processes and the surface energy budget for this climate–sensitive region. Leveraging high–resolution Himawari–8 satellite brightness temperature data, C–band radar observations, and BARRA–R2 regional reanalysis, a multi–year analysis is conducted across three representative zones: coastal land, coastal ocean and open ocean. Results show that diurnal cycles vary distinctly by region and are strongly modulated by prevailing wind regimes. In general, westerly regimes are associated with clear skies and stronger daytime heating over the coastal ocean with enhanced convection over coastal land. In contrast, the frequently observed southeasterlies lead to relatively weaker development over the land and ocean. Cloud and rainfall maxima exhibit out–of–phase behavior between land and ocean, with rainfall often preceding cold cloud tops, indicative that cold brightness temperatures frequently correspond to decaying anvils rather than active convection. Latitudinal and topographic differences contribute to more intense convection near Cairns than Townsville. Variations in inland versus offshore propagation speeds further highlight regional complexity. Our findings emphasize the need for high-resolution simulations to better understand the convection initiation and propagation processes that shape cloud cover and rainfall variability over the GBR during the coral bleaching season, when cloud-radiation interactions may influence reef heat stress.

1 Introduction

Variations in the diurnal cycles of clouds over tropical regions significantly influence rainfall variability and regional heat and energy budgets. Over the Great Barrier Reef (GBR), the relationship between local–scale cloud cover and radiation is a key factor modulating the sea surface temperatures (SSTs) (Huang et al., 2024; Leahy et al., 2013; McGowan and Theobald, 2023;

Richards et al., 2024, 2026; Zhao et al., 2022). Through its modulation of incoming solar radiation and outgoing longwave radiation, cloudiness can influence the timing and magnitude of upper-ocean warming, which is a key factor in the development of thermal stress conditions associated with coral bleaching events (CBEs). Given that anomalously warm SSTs are the main driver of mass CBEs, improved understanding of the spatial and temporal variability of cloud systems in this region is a critical step toward improving our understanding of the atmospheric contribution to reef-scale thermal conditions. In particular, characterizing the formation, propagation, and dissipation of cloud systems provides important context for interpreting atmospheric variability experienced by the GBR during the austral warm season.

Driven by the daily cycle of solar heating, diurnal cycles not only impact local and regional weather, but can also contribute to non–linear upscale processes which can influence the global climate (Masson et al., 2012; Slingo et al., 2003). This effect is particularly pronounced in the deep tropics where diurnally forced convection and rainfall accounts for roughly 50% of mean rainfall and strongly interacts with the Madden–Julian Oscillation (MJO) (Birch et al., 2016; Love et al., 2011; Rauniyar and Walsh, 2011). Global transport of moisture and energy is intricately linked to tropical variability, prompting extensive research on diurnal cycles, particularly over the Maritime Continent (MC) (Lopez-Bravo et al., 2023b; Mori et al., 2004; Neale and Slingo, 2003; Sakaeda et al., 2017; Yamanaka et al., 2018).

Climate models continue to systematically underestimate mean convection and rainfall in the tropics, often due to deficiencies in how they represent key processes controlling the diurnal cycle. In particular, many models have difficulty capturing the timing, amplitude, and propagation of convection because of limited spatial resolution and parameterized convection schemes that cannot fully resolve the interaction between boundary-layer evolution, surface heating, moisture convergence, and cloud–precipitation feedbacks (Christopoulos and Schneider, 2021; Covey et al., 2016; Tang et al., 2021; Xie et al., 2019). Recent advances in convection-permitting modeling, including emerging regional and a small number of global-scale simulations, have demonstrated substantial improvements in representing the diurnal cycle of convection and its propagation, although such approaches remain at the frontier of computational capability and are not yet widely available for long-term or ensemble climate applications (Clark et al., 2016; Hohenegger et al., 2008; Huang et al., 2026; Kendon et al., 2019; Pearson et al., 2014; Stevens et al., 2019). This underscores the critical need to understand local–scale convective processes, particularly in under–studied regions such as northeast Queensland, Australia (Birch et al., 2016; Love et al., 2011; Neale and Slingo, 2003).

Diurnal cycles of clouds and rainfall over tropical coastal land regions, particularly in the nearby MC, typically peak during the afternoon–to-early evening (Lopez-Bravo et al., 2023b; Hassim et al., 2016; Mori et al., 2004; Vincent and Lane, 2016; Yang and Slingo, 2001). These patterns are shaped by local–scale processes such as sea and valley breezes, and boundary layer mixing, which are further influenced by local topography and large–scale background wind fields (Bui et al., 2023; Dao et al., 2025b; Pereira and Rutledge, 2006; Short et al., 2019). Convection that develops over land during the day often propagates offshore during the evening and night, leading to peak cloudiness and rainfall over adjacent ocean areas during the late evening to early morning hours (Lopez-Bravo et al., 2023b; Yang and Slingo, 2001). High–resolution simulations show that offshore propagation can extend up to 700 km from the coastline (Vincent and Lane, 2016), and is associated with two distinct mechanisms: slow–moving density currents associated with the land and mountain breezes near–shore, and faster–traveling gravity waves beyond 200 km from the coastline (Mapes et al., 2003). While these patterns represent typical diurnal behavior in tropical coastal and marine environments, significant regional variations exist (Lopez-Bravo et al., 2023b; Peatman et al., 2023; Yokoi et al., 2017). Therefore, it is essential to characterize the diurnal cycles of clouds and rainfall specific to the GBR region, which spans both tropical and subtropical zones, and is subject to strong gradients in large-scale circulation, thermodynamic conditions, and coastal–oceanic interactions.

Understanding the diurnal variability of local cloud and rainfall cycles is crucial for uncovering how cloudiness interacts with surface energy fluxes, and for identifying the processes that govern these exchanges. Vincent and Huang (2022) examined the relationship between local morning insolation and the diurnal rainfall cycle for three forested sites in the MC. They found that higher morning insolation is associated with increased afternoon rainfall over land, and that this was poorly captured in convection–permitting model simulations. Beyond the MC, relatively few studies have explored how diurnal cycles of clouds and rainfall interact with the boundary layer and surface fluxes. May et al. (2012) used data from the international Tropical Warm Pool International Cloud Experiment (TWP–ICE) and weather radar (among other instruments) to investigate the effects of convective rainfall on surface radiation in a coastal monsoon setting. Their findings showed that the shortwave (SW) cloud effects dominated net surface radiation fluxes, with up to three times more energy reaching the surface during periods of large–scale suppressed conditions. In contrast, during the monsoonal period, increased cloud optical thicknesses and persistent high–level clouds significantly reduced net surface radiation by blocking incoming SW radiation. Direct in situ measurements of the surface energy balance are far more common over land than ocean, largely due to the logistical challenges of instrument setup and maintenance in marine environments. In the southern GBR, a case study by McGowan et al. (2010) examined the surface energy balance using in situ measurements. They found that 80–98% of net daytime radiation reaching the ocean surface contributed to heating of shallow reef flats. Although their observations were limited to spring and winter, the study highlighted the critical role of cloud cover in modulating the ocean heat budget.

In the context of clouds and rainfall over the GBR, Zhao et al. (2022) provided a broad characterization of seasonal cloud properties which are influenced by local-scale forcings across large spatial scales. More recently, Dao et al. (2025a) investigated wet-season rainfall propagation over northeast Queensland using a 180-day convection-permitting regional model simulation complemented by radar observations around Townsville. Their results demonstrated that interactions between land–sea breezes and large-scale background winds play a key role in regulating coastal rainfall patterns, particularly the offshore and onshore propagation of heavy rainfall systems. These studies highlight the importance of multiscale interactions in shaping coastal convection in the region. However, a more integrated understanding of diurnal cloud and rainfall evolution across coastal and marine environments remains needed to better characterize regional variability and its implications for coral bleaching risk.

Building on this scope, we examine the diurnal variability of both clouds and rainfall during the Coral Bleaching Season (CBS) using multi-year Himawari-8 observations, BARRA-R2 regional reanalysis, and rainfall observations from three coastal radars. Unlike Dao et al. (2025a) which focused primarily on rainfall propagation, we consider the coupled evolution of cloud and rainfall systems across coastal land, coastal ocean, and open ocean environments under different prevailing wind regimes, with a particular emphasis on the spatial and temporal variability of cloud-top characteristics, rainfall timing, and cloud–rainfall relationships associated with convection across northeast Queensland including the GBR. This study therefore addresses two primary scientific questions: (1) What are the characteristics of the diurnal cloud and rainfall cycles over coastal and open ocean regions of north–east Queensland? (2) How do the background wind fields interact with local–scale processes to shape these diurnal patterns? Focusing on the CBS period (January–April), when most CBEs in the GBR occur, we combine satellite, radar, and regional reanalysis datasets to characterize the diurnal variability of cloud and rainfall and examine the thermodynamic and dynamical factors that modulate them. Through this integrated analysis, we propose plausible mechanisms underlying the observed cloud and precipitation variability, providing a foundation for future targeted process studies.

2 Data and Methods

2.1 Observational and Reanalysis Datasets

Cloud diurnal cycles were analyzed using the Channel 13 Brightness Temperature (BT; infrared wavelength band 10.4 μm) from the Himawari–8 satellite Level 1 atmospheric and cloud property dataset, which covers the Australian region at an hourly temporal and 2 km spatial resolution (Lopez-Bravo et al., 2021a, b). The BT data was regridded for the study domain at 2 km spatial resolution, spanning 21.5°–14° S and 143°–152° E, encompassing a region of north–east Queensland, the central GBR and the Coral Sea, including the coverage areas of three weather radars (Fig. 1). Diurnal cloud characteristics were analyzed for the January to March period — including small convective clouds observable with the high resolution Advanced Himawari Imager (AHI). A shortened Coral Bleaching Season (CBS) was analyzed due to data availability (Jan–Mar rather than the defined CBS Jan–Apr). Previous studies of the same Level–1 dataset have provided detailed insights on diurnal cycles of convection in the tropical Maritime Continent (Lopez-Bravo et al., 2023a, b).

Rainfall estimates were obtained from Level–2 historical ground reflectivity retrievals derived from C–band Doppler radar data. This study uses data from the Townsville, Cairns and Willis Island operational weather radars operated by the Australian Bureau of Meteorology, archived on the National Computational Infrastructure (Soderholm et al., 2022). Historical ground reflectivity data has spatial resolution of 1 km, extending horizontally from the radar site up to a range of 150 km in all directions (360°), with a temporal resolution between 5–10 min (increasing in frequency towards the end of the analysis period). The analysis focuses on the full CBS (Jan–Apr), for the years when data from for all three radars are available (2012–2022).

Surface wind data from the Australian Bureau of Meteorology's automated weather stations (AWS) in Townsville and Cairns are used to highlight the complex local–scale influences on surface conditions. AWS data was analyzed for the full CBS for the period of 1990 to 2020, with a temporal resolution of 30 min. The location of both stations is shown in Fig. 1, with height above sea level of 4.34 m for Townsville and 2 m for Cairns (with wind measurements 10 m above ground level). Hourly averaged wind direction was calculated using the circular mean, which is used for averaging angular data (i.e. taking the average of 350° and 10° to result in 0°).

The Australian Bureau of Meteorology Atmospheric high–resolution Regional Reanalysis for Australia (BARRA–R2) was used to provide meteorological context for the radar rainfall and satellite cloud observations. BARRA–R2 covers the Australian region from 1979 to the present, with a horizontal grid resolution of 12 km and a temporal resolution ranging from hourly to monthly; this study focuses on variables at hourly resolution. Full documentation can be found in Su et al. (2022). Previous studies have used the BARRA–R2 reanalysis to examine diurnal cycles of temperature and humidity over northern Australia

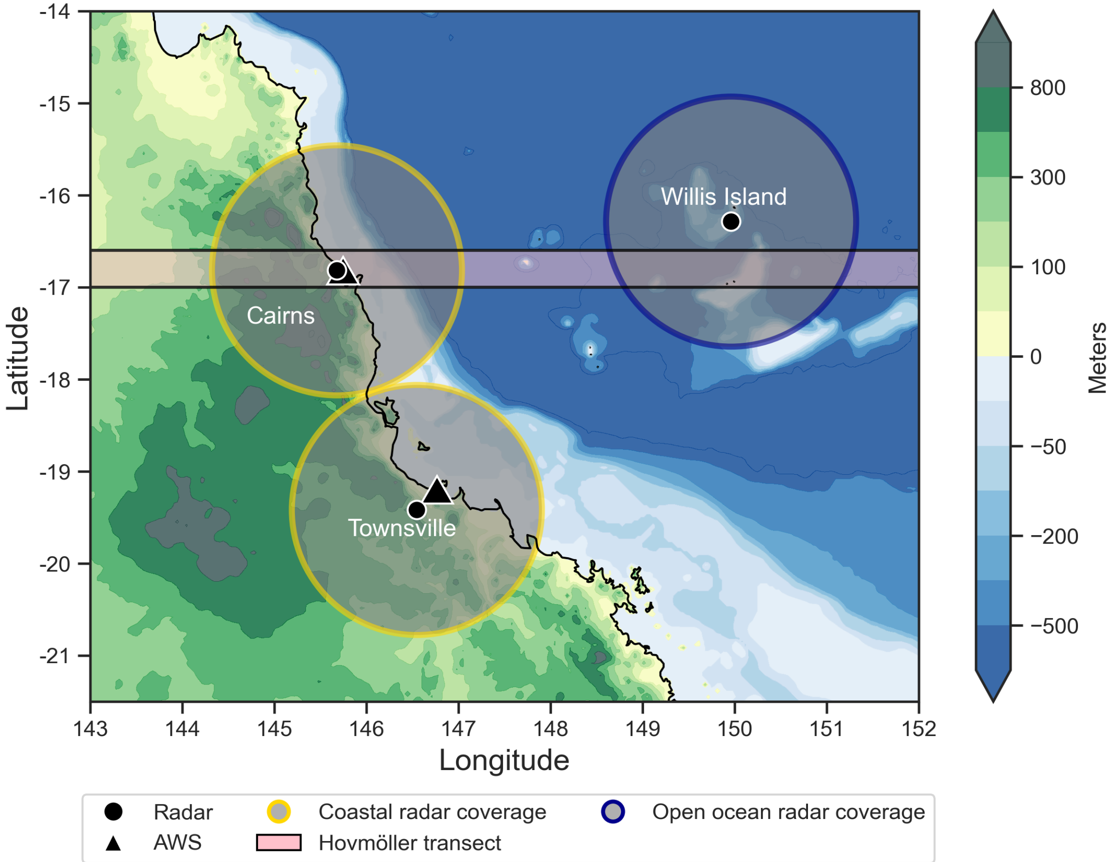

Figure 1. Map of the study domain, including elevation above and below sea level for north–east Queensland produced using the NOAA ETOPO2 dataset (NOAA National Geophysical Data Center, 2006). Shown is the complex coastal topography, shallow coastal oceans of the GBR with reef locations (Lawrey and Stewart, 2016), and the deep bathymetry of the open ocean. Townsville and Cairns Automated Weather Station (AWS) locations are marked by black triangle markers. The three large gray circles show the spatial coverage of the Townsville, Cairns and Willis Island radars, with black circle markers indicating the radar site location. Defined coastal and open ocean regions are indicated by the yellow and navy radar domain colours respectively (the coastline in black divides coastal land and ocean regions). Hovmöller analyses (see Section 2.2) were conducted over the pink shaded zonal transect.

(May et al., 2022). The higher horizontal resolution of BARRA–R2 compared to global reanalyses enables improved representation of local features such as coastal and topographic circulations, though fine–scale processes (such as convection) remain parametrized.

2.2 Methods

In this study, BARRA–R2 was used primarily for defining the background wind and local environmental conditions through composite analysis. Large-scale meteorological conditions were characterized by 850 hPa level winds, whose direction and strength relative to the coastline have been shown to influence the diurnal cycle of coastal precipitation (Aoki and Shige, 2024; Dao et al., 2025a; Peatman et al., 2021). The mean 850 hPa wind direction at 12 Local solar Time (LT) from BARRA–R2 was calculated across each radar domain for the full CBS from 2012 to 2022. For each day within the temporal domain the 12 LT mean wind direction was computed (by first averaging zonal and meridional components separately before computing wind direction), and each hour of that day (00-23 LT) assigned to the resultant wind regime. In this way composite results are reflective of a full diurnal cycle. Wind regimes at 850 hPa were categorized as north–easterly (0°–90°), south–easterly (90°–180°), south–westerly (180°–270°) and north–westerly (270°–360°). This classification was designed to establish a clear northerly–southerly distinction, effectively separating tropical air masses (typically warmer and more humid) from those of mid–latitude origin (typically cooler and drier). Due to the variation in coastline orientation across the radar domains, a simple easterly–westerly division was also adopted to ensure consistency and interpretability in the analysis.

To better understand the convective environments associated with each wind regime, the thermodynamic structure of the atmosphere was examined using vertical profiles of equivalent potential temperature (θ_e). Profiles were constructed at the BARRA-R2 grid point nearest to each radar site (Townsville, Cairns, and Willis Island), using temperature and specific humidity fields across all pressure levels, calculated using the open-source MetPy Python package. θ_e is a combined measure of temperature and moisture, and it provides a useful indicator of an air parcel's convective potential. Higher values of θ_e suggest warmer or more moisture–rich conditions, whereas lower values are associated with colder or drier conditions. The vertical structure of θ_e also reveals information about boundary layer depth and stability, taking into account latent heat release from condensation of the moisture in the air. Analysis of θ_e anomalies associated with each wind regime was done by constructing a smoothed rolling mean climatology with a 31 day centered window (for the period 1979-2024 Jan-Apr) to remove seasonal signals.

Instantaneous rain rate (R mm h^{-1}) was derived from the historical ground radar reflectivity factor (Z mm^6 m^{-3}) using the Z-R relationship, $Z = aR^b$. Constants a and b used in this study (see Appendix A Table A1 for values) are estimated by Pudashine et al. (2026) using rain gauge observations near each radar site. The exception to this is the Willis Island radar, which does not have a co-located in situ rain gauge for calibration (Bowden et al., 2024), and also exhibits the highest proportion of missing temporal data (6.65% of times analyzed), and is therefore associated with larger uncertainty. Prior to the diurnal analysis, the rain rate data required pre–processing to remove regions with erroneous data caused by the partial radar beam blockage from complex topography around the Townsville and Cairns radar sites. To identify regions with erroneous rain rate data, the climatological mean rain intensity over 2012–2022 was calculated, and a lower threshold was applied to exclude affected data from the diurnal analysis. No lower threshold was applied to the Willis Island radar data, as the highest elevation on the island is 20 m above sea level and topographic blockage is absent.

Diurnal cloud and rainfall analyses focused on three distinct regions: coastal land, coastal ocean and open ocean, as indicated in Fig. 1. Coastal land is defined as land areas within the Cairns and Townsville radar domains, while coastal ocean encompasses the oceanic portions of these radar domains. These regions were delineated using land–sea masks derived from the National Oceanic and Atmospheric Administration (NOAA) 2–minute Gridded Global Relief Data (ETOPO2) v2 dataset, which provides high–resolution topography, bathymetry and shoreline information (NOAA National Geophysical Data Center, 2006). In this classification, coastal ocean areas are defined by surface elevation below 0 m ($z < 0$) and coastal land by elevation above 0 m ($z \geq 0$). The open ocean is defined as the area within the Willis Island radar domain. Given that Willis Island lies about 450 km from the Queensland coastline, and measures only about 500 m in length and 150 m in width, it is considered to have little to no land–surface influences on local convection and rainfall processes.

The diurnal mean hourly values of cloud BT, rain intensity and rainfall frequency across the CBS were computed for each of the three regions — coastal land, coastal ocean and open ocean — under the defined wind regimes. Rain intensity and frequency were calculated using a ±30–minute window around each hour to match the hourly temporal resolution of the cloud BT dataset. Rain intensity calculations include all time periods (i.e. raining and non–raining) to maintain consistency with BT diurnal cycles. Rain frequency was defined as the percentage of points in a given time step where rain rate was greater than 0.1 mm h^{-1}. An example of satellite–derived channel 13 BT and corresponding radar rain rate retrievals at a single time step over the Cairns radar domain is provided in Fig. 2.

The diurnal evolution of cloud and rainfall was examined through a Hovmöller analysis. A zonal transect was chosen which spans the coastal land, coastal ocean and open ocean regions (shown in pink in Fig. 1). This transect crosses both the Cairns and Willis Island radar domains, offering simultaneous data on cloud and rainfall characteristics for coastal land, coastal ocean and open ocean regions. Mean hourly values of BT and rain intensity were calculated for each longitude point along the transect using a narrow latitude range (16.6°–17° S), to minimize radar–induced noise. These data were used to generate Hovmöller diagrams that represent the mean diurnal cycle of each variable and reveal patterns in the spatiotemporal propagation of cloud and rainfall features across the domain.

3 Results

3.1 Background wind regimes

The large–scale wind regimes during the CBS period play a crucial role in shaping local thermodynamic environments and convective behavior. This section examines the characteristics of the four wind regimes (850 hPa winds) defined in Section 2.2. Figure 3a shows histograms of the 850 hPa winds for each regime at the three study sites, while the monthly frequency distribution is presented in Fig. 3b–d. Additional statistical summaries are provided in Appendix A Table A2.

The south–easterly wind regime, representing the trade winds, dominated across all three sites, accounting for 57-67% of the CBS period. At Townsville, south–easterly winds were least frequent in January (about 50%) but increased steadily to 75% by April. Cairns and Willis Island show relatively similar frequencies in January–February followed by a marked increase

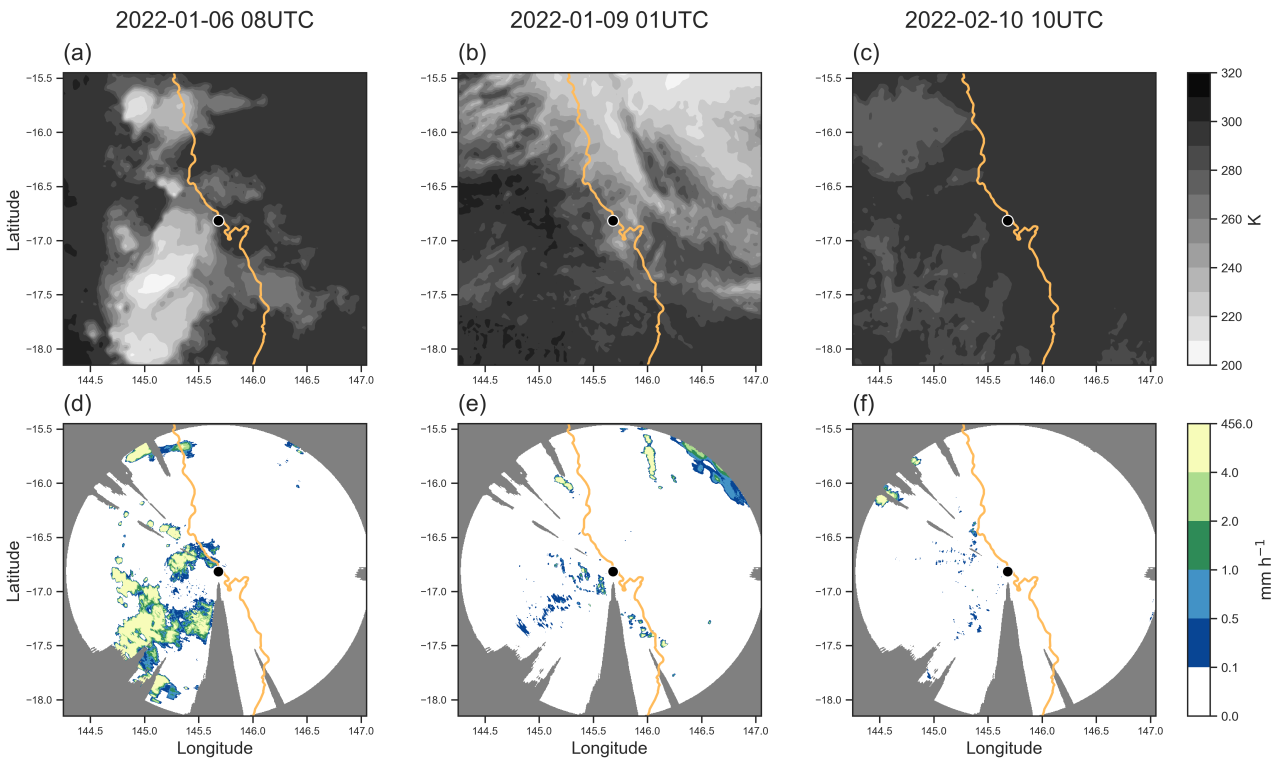

Figure 2. Snapshots of the cloud fields from satellite channel 13 BT and Cairns radar rain rate fields in UTC for: (a,d) 2022-01-06 0800; (b,e) 2022-01-09 0100; and (c,f) 2022-02-10 1000. All plots show the Cairns radar domain, with the Queensland coastline shown in orange (land on left). Black markers indicate the Cairns radar site location. Cloud BT is shown in filled gray–scale contours where white indicates colder BTs, and black indicates warmer BTs. Rain rate in (d,e,f) is shaded in color, with dark gray shading indicating regions where no observations are taken (i.e. the corners of the Constant Altitude Plan Position Indicator radar retrieval grid) or masked (due to radar beam blockage).

in March and April. This north–south contrast may reflect stronger tropical influences at the lower–latitude sites early in the season, and a progressive strengthening of the trade wind belt as the Inter–Tropical Convergence Zone (ITCZ) shifts northward.

The north–easterly wind regime was the second most common regime across all three sites during the CBS, occurring 15-23% of the time. It was most commonly observed in January and February over Townsville (31.5% and 27.6% respectively). Cairns and Willis Island exhibit less month–to–month variation in north–easterly frequencies (19.1–20.3%) during the same period of time, with a similar drop–off from March onward (Fig. 3c, d). This regime's seasonal decline coincides with the strengthening south–easterlies, indicating weakening of tropical influences.

North–westerly and south–westerly regimes were relatively infrequent, each occurring in 6-13% of CBS periods, with peak frequencies during January–February and a marked decline by April. South–westerlies became especially rare at Willis Island in April (3.3%). While the northwesterly regime is likely associated with transient tropical lows, monsoonal flow, or monsoon burst events (Wheeler and McBride, 2012), the south–westerly regime is likely more closely linked to the passage of cold

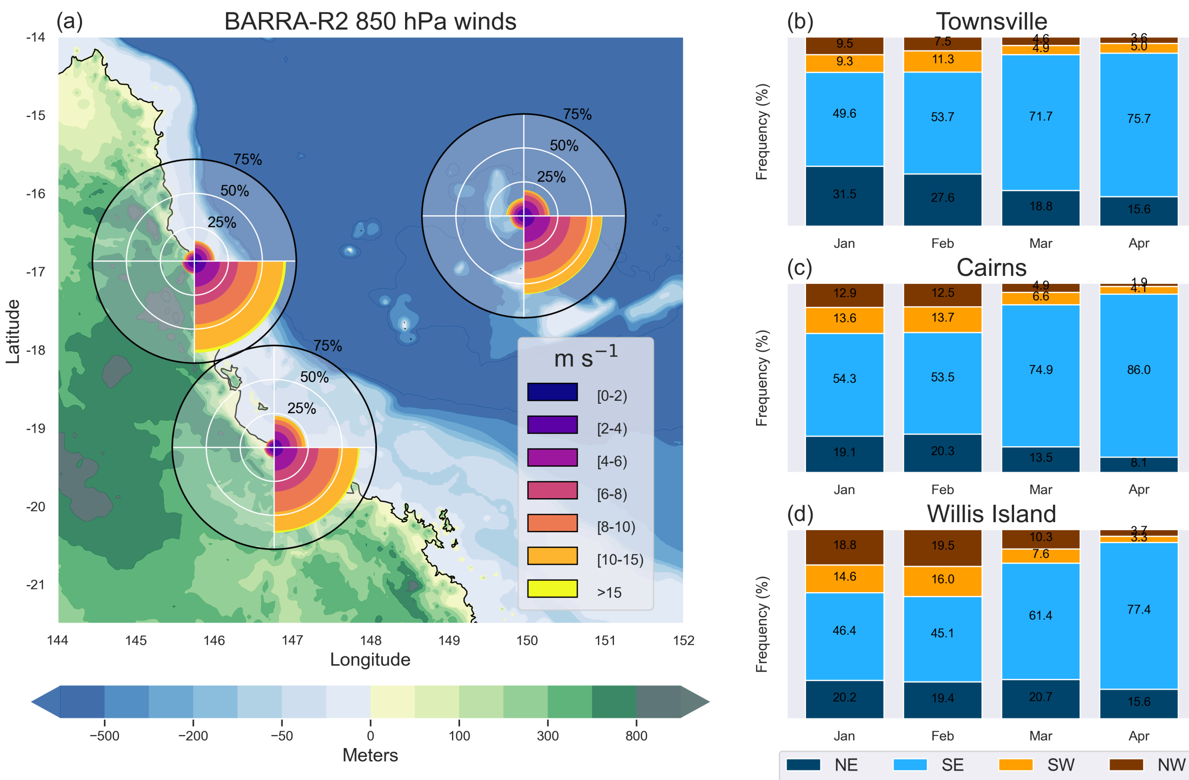

Figure 3. (a) Polar histograms over the CBS for BARRA–R2 850 hPa wind regimes defined in Section 2.2. Bar length indicates wind direction frequency, and colours indicate the corresponding wind speeds in m s^{-1}. (b,c,d) shows the monthly regime frequency for Townsville, Cairns and Willis Island. BARRA–R2 850 hPa winds are averaged over each site's radar domain (see Fig. 1) for the CBS over the period 1979–2024.

fronts driven by deep mid–latitude troughs along the east coast (Kong and Zhao, 2010). The enhanced westerly flow and deep convection typical of north–westerlies are also consistent with active MJO phases influencing northern Australia (Dao et al., 2023).

In summary, south–easterly trades dominate the CBS period, with a clear seasonal transition replacing early–season tropical and cyclonic regimes — which drive the higher frequency of northerlies (Richards et al., 2026). Latitudinal differences suggest stronger tropical influence at Cairns and Willis Island, particularly early in the season, likely modulated by MJO activity, monsoon flows and ITCZ positioning.

3.2 Thermodynamic environment

The CBS mean and wind–regime–averaged θ_e profiles for the three sites are shown in Fig. 4a, c, e, with anomalies relative to a smoothed rolling mean climatology shown in Fig. 4b, d, f. The four large-scale wind regimes can be interpreted in terms of two key controls on convective potential: (i) the moisture and temperature characteristics of the air mass (θ_e magnitude), and

(ii) the vertical stability structure (θ_e gradient and inversion strength). To complement the θ_e analysis, corresponding Convective Available Potential Energy (CAPE) and vertical velocity cross-sections from the BARRA-R2 reanalysis are presented in Appendix A (Figs. A1–A2), providing additional insight into the spatial patterns of instability and large-scale vertical motion associated with each regime.

The four wind regimes represent fundamentally different thermodynamic and dynamical environments for convection. The south-easterly regime represents a cool, dry, and highly stable environment, with persistent negative θ_e anomalies through the column. Stronger warming aloft relative to the boundary layer enhances stability above the 600 hPa inversion. This suppression is reflected in uniformly low CAPE, generally below 1000 J kg^{-1} over land and below 1500 J kg^{-1} over the adjacent ocean (Fig. A1d, h). The absence of large-scale ascent over the marine sector further limits opportunities for convective development (Fig. A2d). In contrast, the north-easterly regime is characterized by a warm and moist lower and mid-troposphere, but weak vertical θ_e gradients hence only moderate instability. Despite the moderate CAPE (2000–2500 J kg^{-1}) over the ocean, a pronounced band of deep ascent along the coastal ranges highlights the importance of orographic lifting in triggering convection (Fig. A2b). The interaction of moist north-easterly flow with the steep coastal terrain appears to locally release the available instability, focusing convection along the windward slopes.

The south-westerly regime exhibits a more heterogeneous structure, with weak positive θ_e anomalies over land suggesting some surface-driven destabilization, while open ocean conditions remain close to climatology. CAPE shows a marked land–sea contrast, exceeding 3000 J kg^{-1} over the coastal ocean but remaining substantially lower further inland (Fig. A1c, g). Localized ascent along the windward coastal ranges highlights the importance of orographic forcing (Fig. A2c). However, the ascent is weaker than in the north-easterly regime, likely because the south-westerly flow encounters less abrupt upwind terrain. As a result, convection is likely influenced more by land surface heating and boundary-layer growth than by orographic lifting alone. By contrast, the north-westerly regime stands out as the most convectively favorable, with strong positive θ_e anomalies in the lower and mid-levels and enhanced vertical gradients indicative of an unstable air mass. CAPE exceeds 2000–3000 J kg^{-1} across much of the domain and is accompanied by deep, widespread ascent (>0.02 m s^{-1}), demonstrating that both thermodynamic instability and large-scale dynamical forcing support convection. This structure is consistent with monsoonal or tropical intrusions that inject warm and moist air masses, providing both moisture supply and reduced stability (Berry and Reeder, 2016). Together, these characteristics highlight how large–scale flow direction modulates both the source characteristics of air masses and the vertical thermodynamic structure that governs convective potential across the study region.

The diurnal evolution of θ_e under each wind regime is shown in Fig. 5 as anomalies relative to a smoothed rolling mean climatology over the CBS. Consistent with Fig. 4, the wind regimes primarily define the background thermodynamic state, setting the moist static energy and stability structure. In particular, north-westerly flow is associated with the highest θ_e, and weakest stability, north-easterly flow shows intermediate moistenining, and south-easterly flow is characterized by persistently low θ_e and enhanced stability. Figure 5 further shows how this background state is modulated by the diurnal cycle.

A clear contrast emerges between the coastal land sites (Townsville and Cairns) and the marine site (Willis Island). Over land, θ_e profiles exhibit strong diurnal modulation of the lower troposphere, especially under north–westerly regimes (Fig. 5a, f). Positive θ_e anomalies larger than 6 K occur during the afternoon and early evening, reflecting daytime surface heating and boundary-layer deepening, which enhance near-surface moist static energy and convective potential. Townsville shows the strongest response under north–westerly flows, consistent with more intense land–surface forcing under this regime. Cairns exhibits a similar but slightly more muted behavior except under south-easterly conditions, where the diurnal signal is substantially suppressed (Fig. 5f, g, h). In contrast, Willis Island shows little systematic diurnal variability across all regimes, indicating that the absence of strong land surface forcing limits sub-daily modulation of θ_e in the marine boundary layer (Fig. 5k, l, m, n). This sharp land–sea contrast highlights the dominant role of surface heating in driving diurnal thermodynamic variability. Overall, these features underscore the interplay between large–scale flow direction and surface type in shaping diurnal thermodynamic evolution and the likelihood of convective activity.

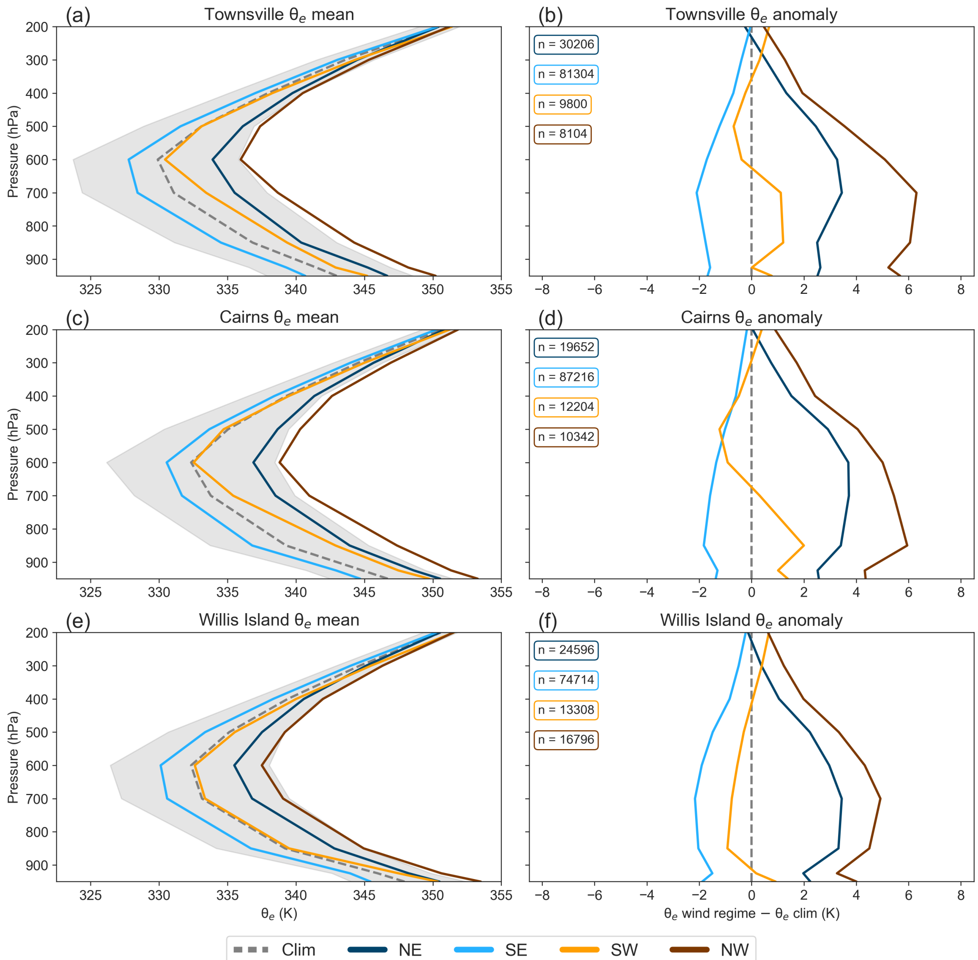

Figure 4. Mean and anomaly θ_e profiles for Townsville (a,b), Cairns (c,d) and Willis Island (e,f) radar sites under each wind regime (north–easterly: NE, south–easterly: SE, south–westerly: SW, and north–westerly: NW) for the CBS over the period 1979–2024 from BARRA–R2. Anomaly plots are calculated by subtracting a smoothed rolling mean climatology from each timestep within the wind regime-classified periods, then averaging across all time steps within each regime to remove seasonal signals. Sample sizes for each site across all times are provided for each regime. Grey shading indicates the inter-quartile range of the θ_e profile.

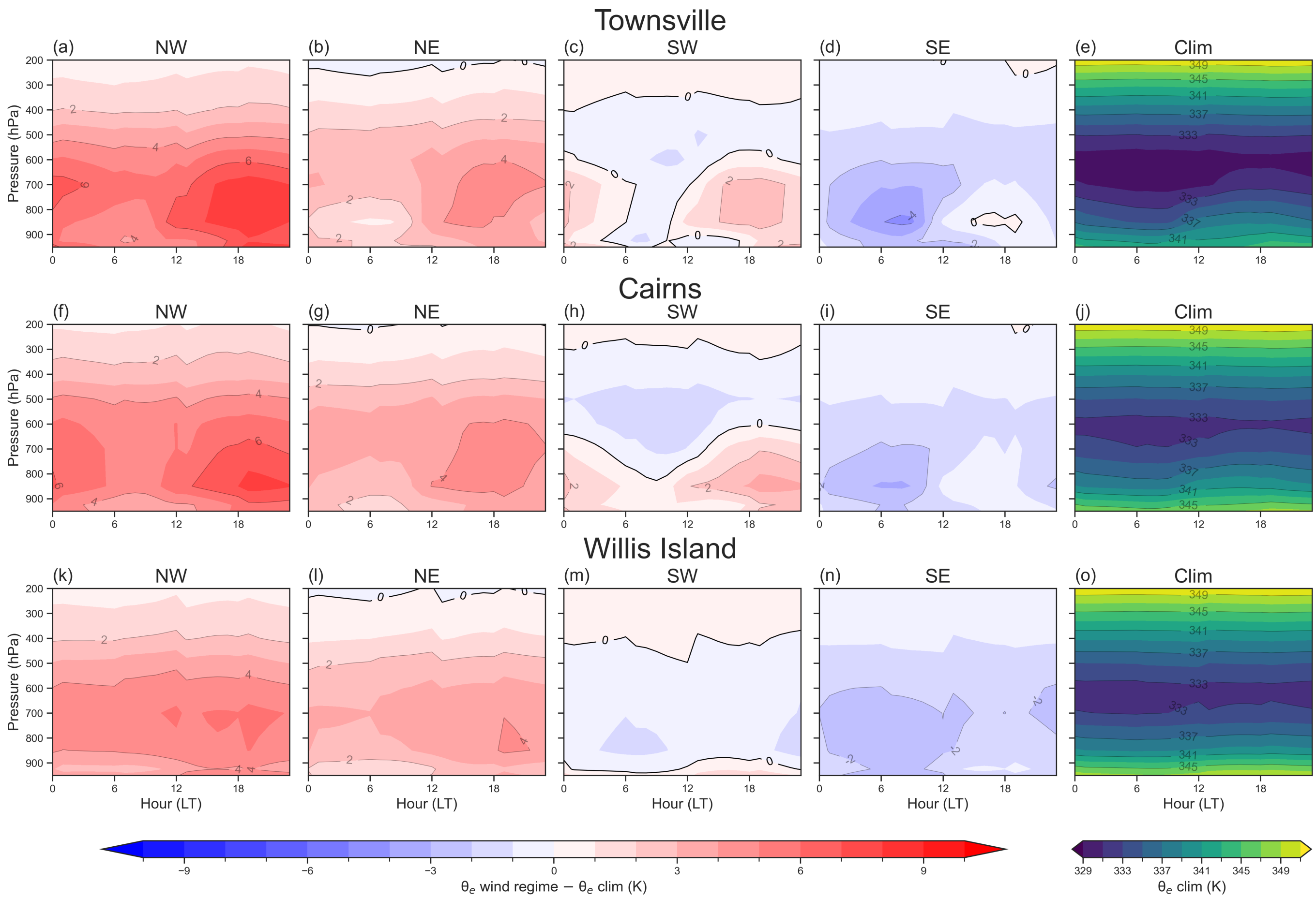

Figure 5. Diurnal θ_e profile difference plots between wind regimes and a smoothed rolling mean climatology over the CBS for (a,b,c,d) Townsville, (f,g,h,i) Cairns, and (k,l,m,n) Willis Island. (e,j,o) show the CBS mean θ_e diurnal profiles over the period 1979–2024 (Jan-Apr). Note that the 'Clim' panels for each site (e, j, o) represent the CBS climatological mean for reference, and are not equivalent to the smoothed rolling mean used in the difference plots (which varies at daily time resolution).

3.3 Diurnal cloud and rainfall characteristics

Next we examine how these thermodynamic conditions influence the diurnal evolution of cloud and rainfall patterns. In general, differences in vertical stability and moisture content across wind regimes are expected to influence not only the likelihood of convection but also its timing and intensity throughout the day. The mean diurnal cycles of satellite–derived Brightness Temperature (BT) and radar–derived rainfall frequency and intensity under different wind regimes are presented in Fig. 6, with the seasonal mean conditions shown in Fig. 6 m, n, o. BT is used as a proxy for cloud-top height, with colder BTs indicating deeper convection, and warmer BTs suggesting shallow cloud or clearer-sky conditions.

A first-order feature across all regimes is again a strong land–sea contrast in the diurnal cycle. Over land, BT typically increases through the morning and decreases sharply in the afternoon to evening, consistent with boundary-layer growth and the development of deep convection, accompanied by a corresponding increase in rainfall frequency and intensity. Over the coastal ocean, this signal is phase-shifted, with rainfall and colder BTs generally occurring from evening to early morning. In contrast, Willis Island exhibits minimal diurnal variability in both BT and rainfall, reflecting weak surface forcing in a more homogeneous marine environment.

Superimposed on this common structure are regime-dependent modulations that primarily affect amplitude, timing, and convective characteristics. The north–easterly regime is characterized by relatively colder BTs and enhanced rainfall compared to the seasonal mean, especially over land. Cairns experiences the strongest diurnal signals among all three sites, with BTs over land warming through the morning (reaching 277 K at 11 LT) and cooling rapidly into evening (253 K by 18 LT), indicative of vigorous deep convection. Townsville shows a similar warming trend (approximately 1 K per hour) but with more gradual cooling, about half of the rate at Cairns, likely reflecting weaker orographic enhancement. Rainfall frequency and intensity at both land sites closely follow this evolution, peaking in the afternoon–evening, especially at Cairns, with moderate amplitudes of 5% and 0.61 mm h^{-1}. A notable feature is that peak rainfall at 16 LT precedes the coldest BTs by 3 hours, suggesting that the minimum BTs likely reflect the later anvil-dominated stage of convection rather than the peak rainfall phase.

In contrast, the south–easterly regime is characterized by the warmest BTs and the weakest rainfall across all land regions, consistent with shallow, low-topped cumulus clouds and suppressed deep convection. Unlike the north–easterly regime, BT and rainfall diurnal cycles in the south-easterly regime over Cairns and Townsville are more synchronized and subdued, though rainfall intensity over Cairns is slightly enhanced in the afternoon — again likely linked to localized orographic lifting and elevated terrain heating, which can partially overcome the otherwise stable background conditions. Over the coastal and open oceans, both BT and rainfall variability remain weak throughout the day, consistent with stable marine boundary layers dominated by shallow trade-wind cumulus and limited diurnal destabilization.

South–westerly regime exhibits very strong diurnal modulation in both BT and rainfall, suggesting enhanced surface–driven convection. Over land, BTs are largest around midday (296 K at Cairns and 298 K at Townsville), indicating minimal cloud cover, before dropping sharply in the afternoon. Correspondingly, rainfall frequency and intensity are minimal around midday but increase rapidly in the early afternoon, reaching maxima in the late afternoon over land and shifting to early morning over the coastal ocean. Cairns generally experiences more frequent and intense rainfall than Townsville, particularly in the afternoon–evening period. Oceanic regions show comparable rainfall magnitude near the coast, while Willis Island again shows little diurnal variability, reflecting its open–ocean character. These patterns align with the south–westerly regime fostering deeper, more organized convection through localized surface heating and atmospheric destabilization.

The north–westerly regime stands out as the most convectively active, with the coldest BTs and highest rainfall frequency and intensity. Over land, convection deepens through the afternoon, with progressively colder BTs and increasing rainfall. The most intense rainfall over land peaks at 17 LT, whereas peak rainfall frequency and cold BTs lag by 3 hours, again reflecting a transition from active convection to mature and stratiform/anvil-dominated cloud. Over the coastal ocean, strong diurnal structure is evident, with daytime (11–14 LT) BT warming and suppressed rainfall followed by nocturnal intensification. The large amplitudes of cloud and rainfall signals over the coastal ocean highlight the strong diurnal forcing under this regime. In contrast, Willis Island shows only weak signals in both fields, consistent with the open-ocean environment. These features are consistent with enhanced instability associated with elevated θ_e and strong vertical gradients fueled by moist north–westerly inflow. Diurnal patterns over land and coastal ocean reflect surface heating and boundary–layer dynamics.

Overall, the diurnal evolution of brightness temperature and rainfall reflects a consistent interaction between large-scale wind regimes and surface forcing. The wind regimes control the background thermodynamic environment and convective potential, while land–sea contrasts regulate the timing, propagation, and amplitude of the diurnal cycle, with the strongest organization occurring under south-westerly and north-westerly regimes and the weakest under south-easterly trade conditions.

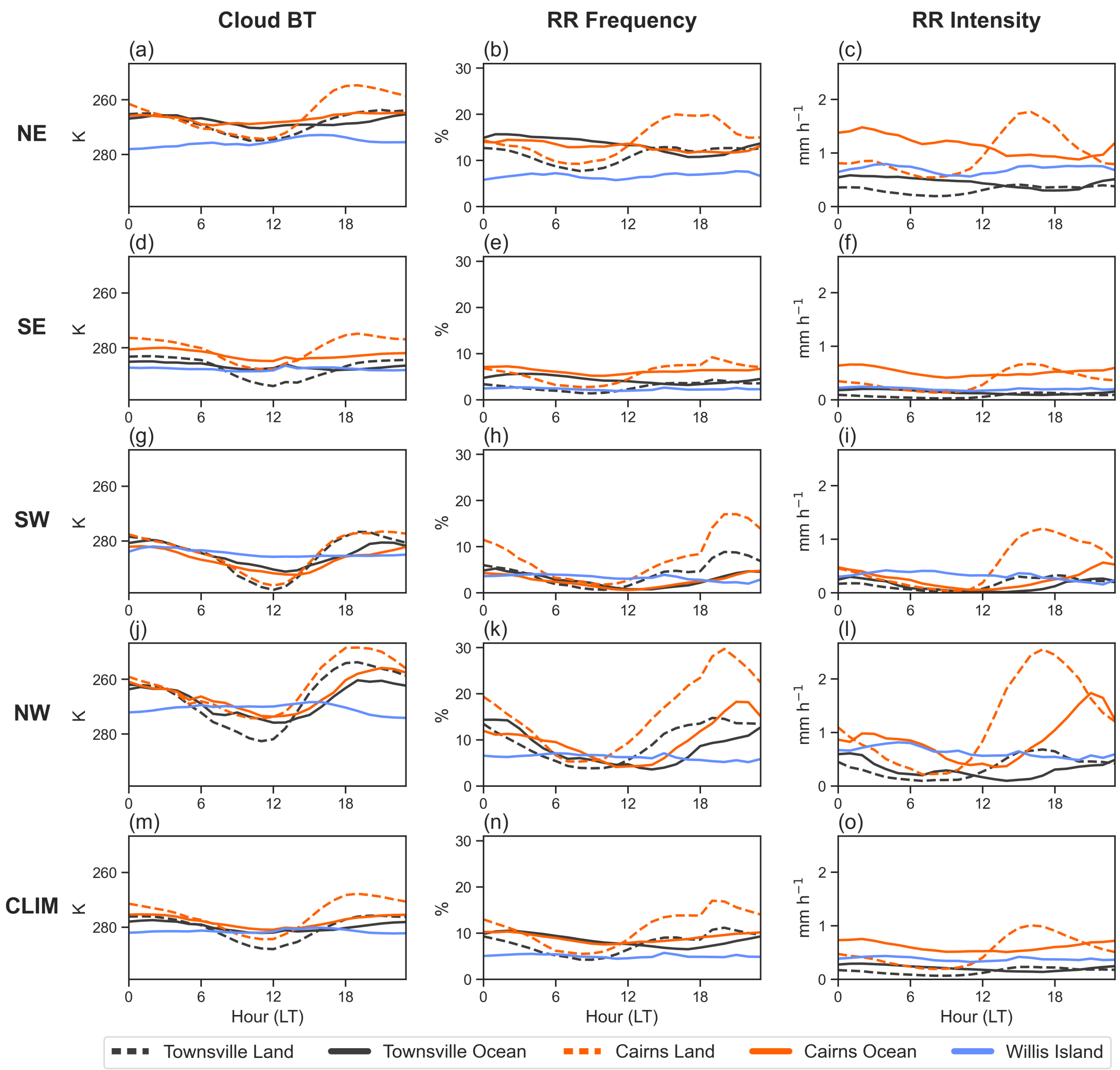

Figure 6. Diurnal cycle of Himawari–8 satellite BT (10.4 μm infrared wavelength band; K), radar retrieved rainfall frequency (percentage of points greater than 0.1 mm h^{-1}) and intensity (mean rain rate mm h^{-1}) calculated over the CBS for each wind regime and site. Each row shows the corresponding BT, rainfall frequency and rainfall intensity with consistent y-axes for each wind regime– with different colored lines for each site. Townsville and Cairns are separated into land (dashed) and ocean (solid) domains, associated with their radar coverage. The BT y–axis is inverted, so that peaks in the diurnal cycle indicate colder BTs. Rain intensity is calculated for all periods of valid data (not just raining periods).

3.4 Spatial structure and propagation

Building on the discussion of diurnal BT and rainfall cycles, Hovmöller diagrams were produced to examine the spatial evolution and propagation of convection through time. Using the method described in Section 2.2, Fig. 7 shows BT and rain intensity (averaged across both raining and non–raining periods) under each wind regime defined by the Cairns domain with terrain elevation in Fig. 7e, f (for reference).

A consistent feature across all regimes is the strong influence of coastal geometry and topography on convective initiation and propagation. Convection typically develops over or near the coastal ranges during the afternoon before propagating either inland or offshore depending on the prevailing background flow. The extent, speed, timing, and organization of this propagation vary substantially between regimes, indicating strong modulation by the large-scale thermodynamic and kinematic environment identified in the previous sections.

The clearest offshore propagation occurs under the north-westerly regime. In this regime, BTs below 253 K develop by 16 LT over coastal land, particularly near regions of elevated terrain (Fig. 7a, e). Nighttime propagation of convection is evident over the coastal and open oceans, with BTs below 263 K reaching 200–300 km offshore, and rainfall extending to the eastern edge of the Cairns radar domain. Inland propagation is comparatively weak in this regime. The coldest BTs are largely confined to near–coastal waters (within 100 km of the coastline) and are associated with relatively slow-moving rainfall features (2–5 m s^{-1}). In contrast, warmer BTs propagate farther offshore more rapidly, at speeds of 12–15 m s^{-1}. In this regime, the coldest BTs correspond closely with the most intense rainfall.

Under the north–easterly regime (Fig. 7b), widespread moderate coastal rainfall persists throughout the day, consistent with a moist environment, while colder BTs (below 263 K) develop over land and adjacent coastal waters during the evening to early morning period. From around 12 LT, BTs below 273 K propagate both inland and offshore, although the inland signal is more coherent and appears more directly linked to coastal convective development. Inland propagation speeds reach approximately 30 m s^{-1}, extending more than 300 km westward from the coastline. The coldest BTs are typically found on the leeward side of the mountain ranges between 19–22 LT, traveling westward — suggesting convection enhanced by mountain effects that produce strong thunderstorms propagating westward into the evening. Offshore propagation is also apparent in the BT field, though this signal is less clearly tied to coastal convection and may partly reflect broader open-ocean cloud variability. Compared to the north-westerly regime, convection appears less organized offshore but more effective at penetrating inland.

For south–westerly regimes (Fig. 7c), coastal rainfall exhibits a pronounced diurnal cycle, with little to no rainfall occurring from early morning through to midday before convection rapidly intensifies during the afternoon. BTs below 283 K form over land during the afternoon before propagating both inland and offshore. The coldest BTs occur between 18–00 LT over land. Early morning convection moves offshore by approximately 100 km, associated with light rainfall. Rainfall contours generally track the BT evolution closely, although peak rainfall (blue) often occurs prior to the appearance of the coldest BTs — again suggesting these may correspond to high–level anvil clouds decoupled from topographic influence.

Under south–easterly regimes, light–to–moderate coastal rainfall is present (similar to north-easterly regimes) but confined to a narrower coastal region. Cooler BTs (283 K) start propagating inland from the coast by 15 LT, penetrating more than 200 km inland at speeds of 12–15 m s^{-1}, with the coldest BTs emerging about 250 km from the coast in the late evening between 20–03 LT, suggesting storm enhancement during inland propagation. Rainfall follows a similar westward propagation, though slightly slower (10–15 m s^{-1}), and generally tracks the BT contours. Compared with the other regimes, convection remains weaker and less spatially extensive, consistent with the more stable trade-wind environment discussed earlier. Localized regions of enhanced afternoon rainfall over elevated terrain further indicate an important role for orographic forcing under otherwise suppressed convective conditions. Over the coastal ocean, convection is less coherent and no strong offshore propagation signal is evident.

The spatial patterns and propagation characteristics of the BTs and rainfall suggest that land–sea breeze circulations play a variable but important role in shaping the diurnal development of convection over north–east Queensland, depending on the prevailing wind regime. Figure 8 presents surface wind roses at 07 and 15 LT, alongside the diurnal evolution of hourly average wind speed and direction at Cairns and Townsville weather stations. We use station-based surface wind observations here rather than the BARRA–R2 reanalysis as the 12 km horizontal resolution of the reanalysis may be too coarse to reliably resolve these coastal circulations. While a classic wind reversal pattern is not observed (likely due to the region's complex coastal geometry and orographic influences), distinct afternoon landward winds indicative of sea–breeze influence are observed at both stations. Similarly, evening seaward winds consistent with land–breeze activity are also evident, supporting the presence of thermally driven circulations despite terrain–induced variability.

Further detail on the variable influence of land–sea breeze circulations can be seen in the contrasting diurnal surface wind patterns observed across different wind regimes at Cairns (Supplementary Fig. A3). Afternoon landward winds are evident across all regimes, though with varying strength, which is a reflection of the modulating effect of background winds and possibly the topographic flows. This variation helps explain the differing speeds and inland reach of the convective propagation seen in Fig. 7, where convection initiates near the coast in the early afternoon and moves inland at speeds characteristic of sea–breeze dynamics. In contrast, seaward winds are most pronounced under the two westerly regimes, aligning with the offshore–propagating convection that peaks in the evening shown in Fig. 7. This suggests a potential role for nocturnal land breezes in triggering marine convection, though the extent of offshore propagation also depends on ambient moisture availability and background wind strength, which influence the distances over which colder BTs are observed.

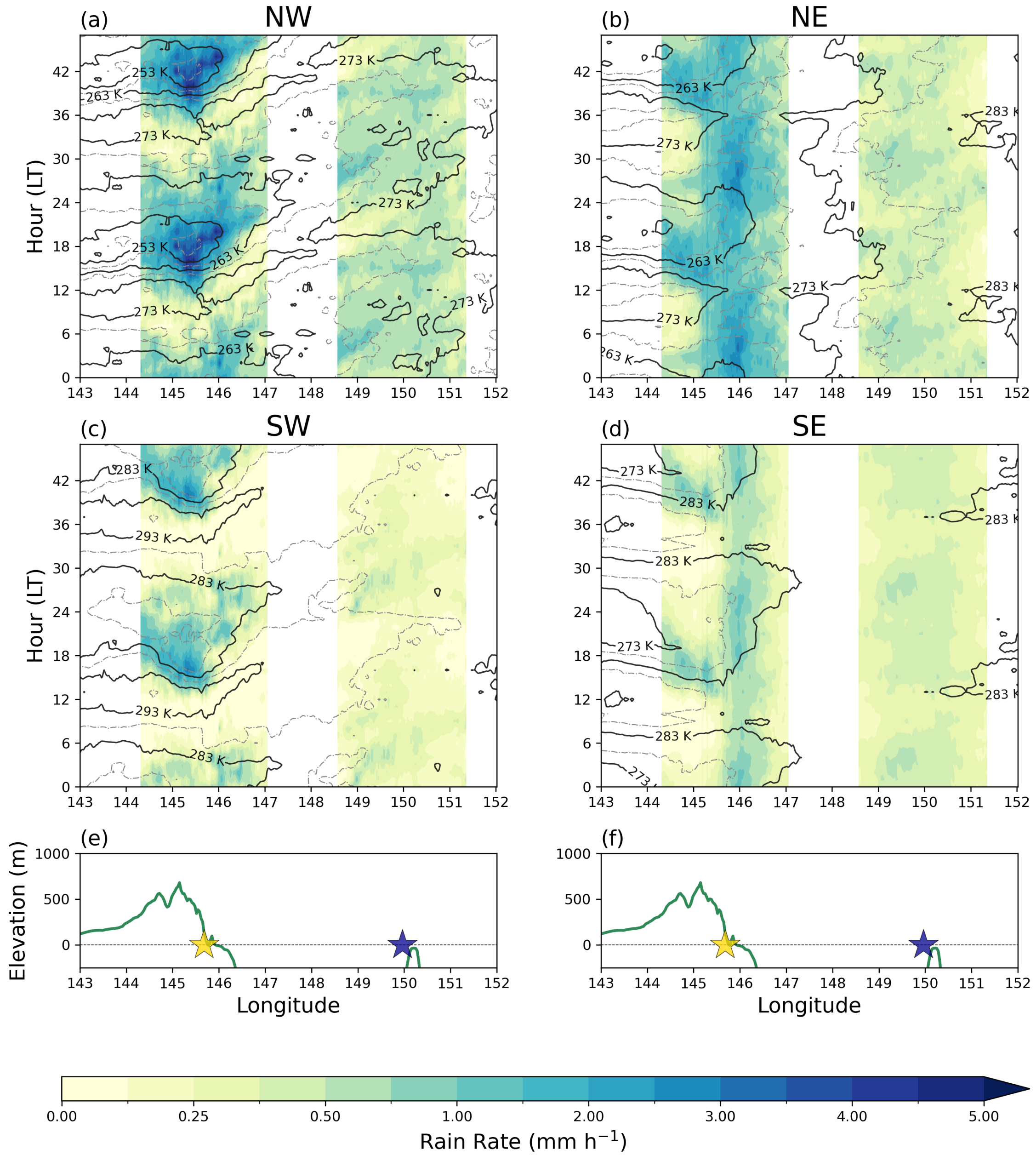

Figure 7. Hovmöller diagrams of cloud BT and rain intensity (including non–raining periods) for the longitudinal transect shown in Fig. 1. (a,b,c,d) show labeled cloud BT contours for 253 K, 263 K, 273 K, 283 K and 293 K (with dashed gray contours every 5 K), along with rainfall data from the Cairns (left filled contours in each panel) and Willis Island radars (right filled contours) under each wind regime. The y axis (in LT) is repeated to show clear propagation of cloud BT and rainfall between the evening and morning. (e) shows elevation from NOAA National Geophysical Data Center (2006) averaged over the longitudinal transect, with this plot repeated in (f) for referral to the above panels. Yellow and blue stars indicate the longitude of the Cairns and Willis Island radar site respectively, with a black dashed line at 0 m elevation.

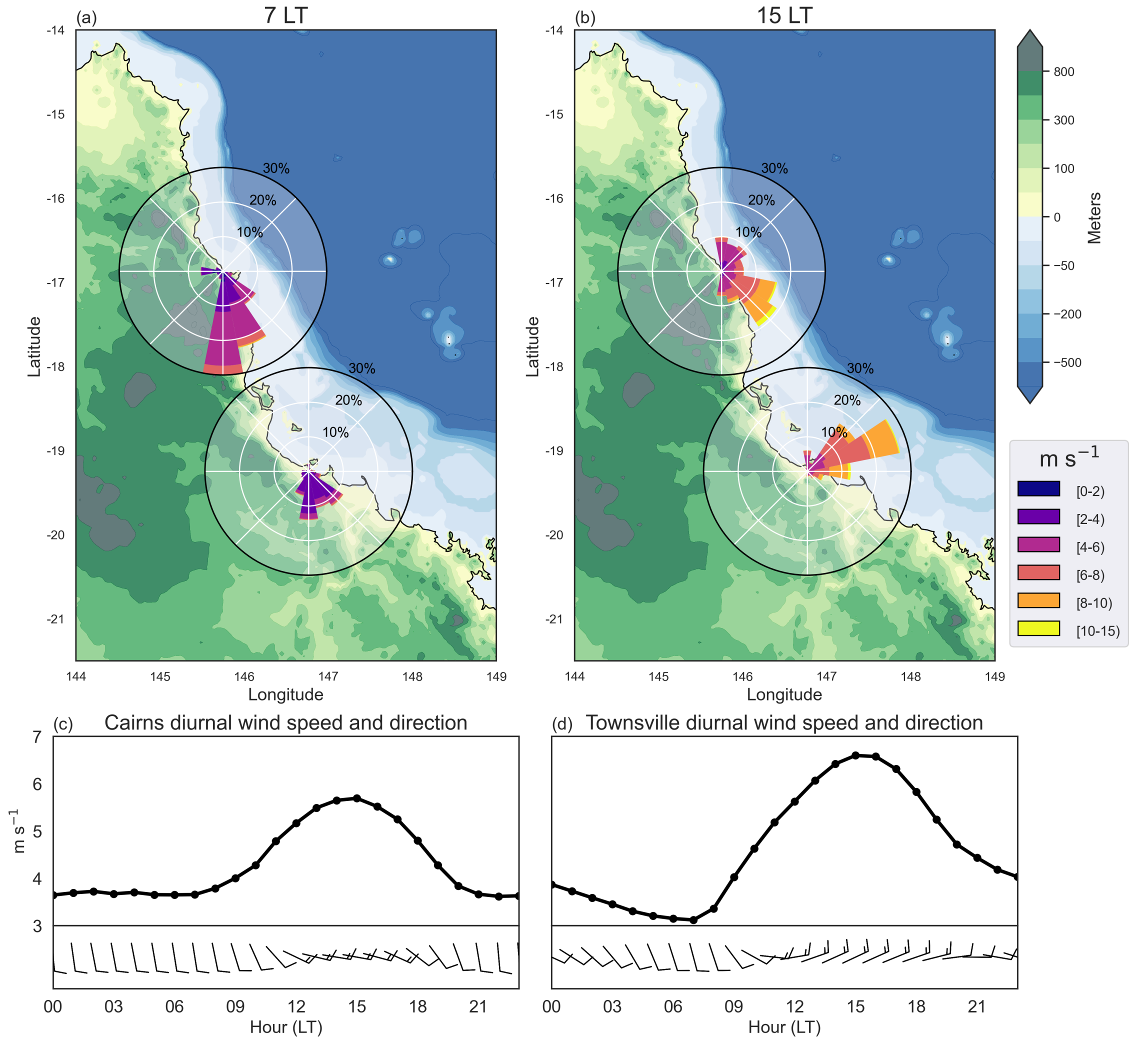

Figure 8. (a,b) Cairns and Townsville AWS surface winds. Wind roses show the surface wind frequency and magnitude at 07 and 15 LT. (c,d) show hourly averaged wind speed and direction (wind barbs; calculated using a circular mean) for each station.

4 Discussion

Our analysis reveals distinct diurnal patterns of convection and rainfall across the Greater GBR region in northeast Queensland Australia, shaped by background wind regimes, geographic features, and atmospheric conditions. Consistent with prior tropical studies (As-syakur et al., 2019; Lopez-Bravo et al., 2023b, 2025; Mori et al., 2004), the coldest cloud tops — indicative of deep convection — are primarily observed over land in the evening, coinciding with the timing of upslope winds from daytime heating and sea–breeze convergence. In contrast, convection over the adjacent coastal ocean peaks later, typically overnight to early morning, propagating offshore at speeds consistent with density currents near the coast and gravity waves further offshore (Dipankar et al., 2019; Lopez-Bravo et al., 2023a; Vincent and Lane, 2016). Notably, the influence of land–sea breeze circulations varies across different background wind regimes, modulating the extent, timing, and propagation of convection.

Figure 9 provides a conceptual summary of the contrasting diurnal cycles of cloud and rainfall, along with the proposed mechanisms of convection initiation and propagation. It is intended as a framework for interpreting the observed diurnal cloud and rainfall behavior, rather than a complete or definitive description of all underlying processes. Some elements are necessarily interpretative, particularly where direct observational constraints are limited, and are therefore presented as hypotheses consistent with the observed patterns and existing literature. The schematic spans five key time periods — nighttime, early morning, morning, afternoon, and evening — and outlines the general evolution of convection and rainfall across the three sites. We also include gravity waves within Fig. 9 which are not fully evidenced in our analysis given the limitation of observations — instead inferred from our estimated convection propagation speeds which are consistent with gravity waves as a mechanism for offshore convection in previous literature (Mapes et al., 2003; Yokoi et al., 2017). These diagrams synthesize well-supported findings from this study with more tentative, literature-informed mechanisms to identify key processes warranting further investigation in future work.

Under the southeasterly regime, weak large–scale forcing and minimal atmospheric instability limit the development of deep convection. As a result, precipitation is dominated by shallow trade wind cumulus producing light, widespread rainfall. Coastal enhancement of convection is persistent, driven by the combined effects of sea breeze convergence and orographic uplift. Diurnal variability is weak, with rainfall occurring sporadically throughout the day.

In the northeasterly regime, warm, humid air masses advected from lower latitudes contribute to elevated equivalent potential temperature. However, despite the abundant moisture, relatively moderate instability and limited buoyancy inhibit the formation of deep convection. Precipitation primarily consists of moderate coastal rainfall, with convection strongly influenced by orographic lifting, as moist north-easterly flow interacting with the steep coastal ranges locally releases the available instability and focuses ascent along the windward slopes. Inland propagation is driven by the diurnal cycle through combined effects of sea breeze circulations and orographic lifting, and offshore propagation likely influenced by gravity wave activity. North–easterly regimes show the largest inland propagation of deep convection, reaching the up wind (western) side of the coastal mountain ranges. The offshore signal, however, is partially obscured by the widespread moisture associated with this regime.

The southwesterly regime promotes deeper and more organized convection, primarily driven by strong localized surface heating and enhanced atmospheric destabilization. This occurs despite the relatively moderate equivalent potential temperature associated with the cooler air masses linked to passing mid–latitude systems. Pronounced diurnal cycles of cloud and rainfall are observed over both coastal land and adjacent ocean, with the sunniest conditions typically occurring from early morning fostering surface heating that initiates afternoon convection.

The northwesterly regime is characterized by the most intense convection, supported by the highest levels of equivalent potential temperature. It exhibits the strongest diurnal variability and produces the heaviest rainfall among the four regimes. Intense precipitation occurs over both coastal land and adjacent ocean, while widespread, persistent moderate rainfall extends across the open ocean. Although inland propagation is less clearly defined, pronounced offshore propagation is evident and appears consistent with a transition from density current outflow to gravity wave–driven processes.

Together, these four regimes highlight the diverse atmospheric conditions influencing clouds and sub–daily rainfall along the Queensland coast. The contrasting roles of large–scale moisture availability, thermodynamic instability, and local forcing mechanisms—such as sea breeze circulations and orographic effects — shape not only the intensity and spatial distribution of clouds and rainfall, but also its diurnal variability and propagation characteristics. Importantly, our results suggest that cloudiness over the GBR cannot be considered solely as a local marine phenomenon. Instead, cloud cover over reef environments is closely linked to the evolution of nearby coastal convection and its subsequent inland or offshore propagation. The differing propagation characteristics among wind regimes imply that the timing, extent, and persistence of cloud cover over the GBR may vary substantially depending on the prevailing large-scale circulation. Given the recognized influence of cloud cover on solar radiation reaching the ocean surface and the links between cloudiness, upper-ocean warming, and coral bleaching risk, these findings provide important context for understanding environmental conditions associated with reef shading during the coral bleaching season.

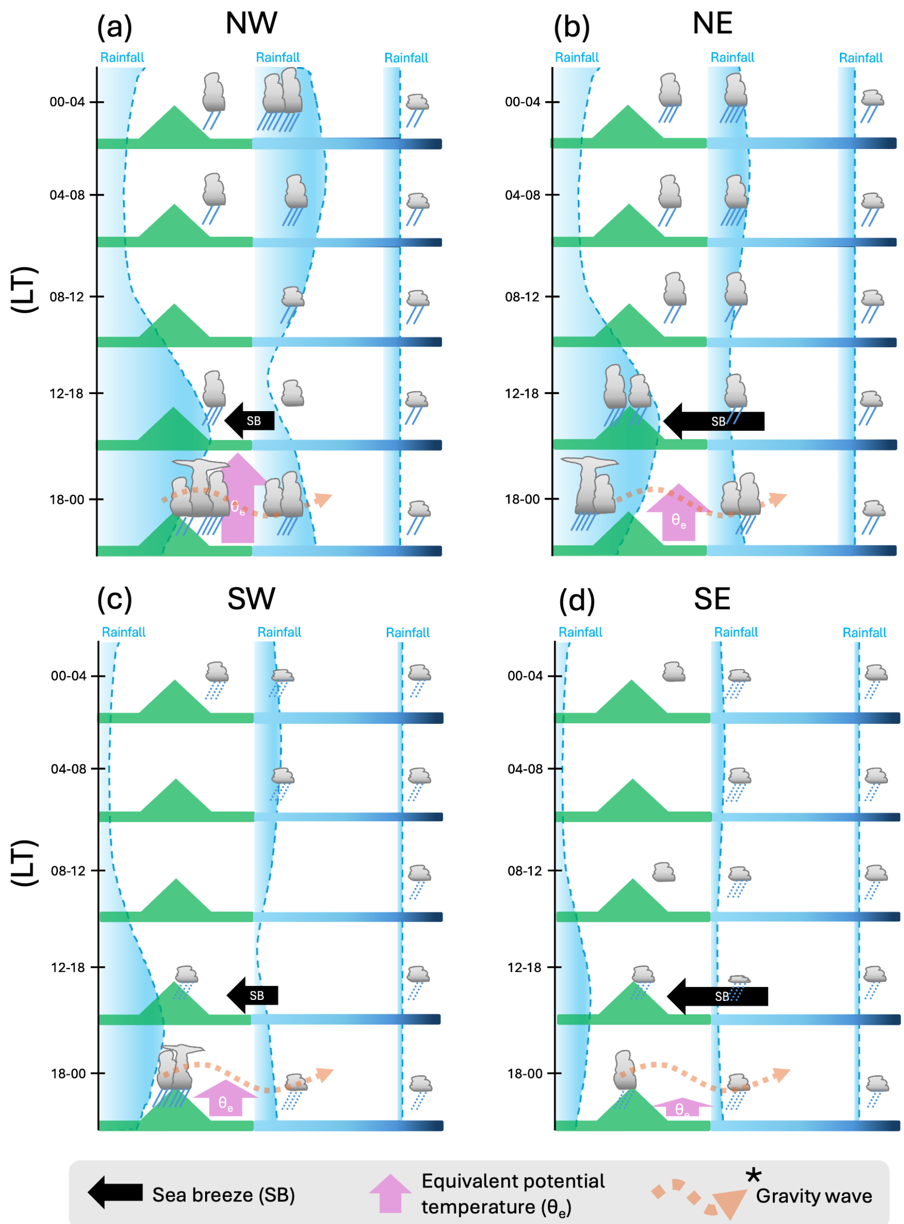

Figure 9. Hypothesized mechanisms for each wind regime (a,b,c,d) cloud BT and rainfall observations. Each panel shows time (Local Time) along the left column, corresponding to mean rainfall changes throughout the day (blue shading). Five distinct stages are shown (nighttime, early morning, morning, afternoon, and evening), with land and topographical features on the left (a general feature of the north–east Queensland coastline), the coastal ocean in the center, and the open ocean on the right. Upward pink arrows indicate the relative size of peak equivalent potential temperatures for each wind regime. The afternoon land sea breeze is shown by black arrows with relative maximum wind speeds indicated by arrow length (see supplementary Fig. A3). *Mechanism inferred from estimated propagation speeds consistent with gravity wave propagation in literature - dashed orange oscillating arrows indicate the nighttime offshore propagation of convection induced by gravity waves.

5 Conclusions

This study characterizes cloud and rainfall diurnal cycles over north–east Queensland during the coral bleaching season, offering a foundation for understanding links between clouds, rainfall, local processes, and surface energy in this climate–sensitive region. Using Himawari–8 data, C–band radar, and BARRA–R2 reanalysis, a multi–year analysis is conducted across coastal land, coastal ocean, and open ocean zones. Key findings are summarized below:

- Background wind regimes significantly modulate diurnal cloud and rainfall cycles by modulating thermodynamic structure and convective dynamics.
- Strongest diurnal cycles occur under westerly regimes over coastal land, with cloud and rainfall variability significantly reduced over the coastal ocean and minimal over the open ocean.
- The southeasterly regime tends to support shallower and weaker convective systems, resulting in reduced cloud development, limited rainfall and little diurnal variability.
- Cloud and rainfall diurnal cycles are out of phase between land and ocean, with peak cloudiness and rainfall occurring in the evening over land and early morning over the ocean.
- Rainfall peaks precede coldest cloud tops over land, suggesting colder cloud tops often reflect anvil cloud remnants rather than active convective cores.
- Latitudinal and topographic influences are substantial, where Cairns experiences more frequent and intense convection than Townsville.
- Convection propagates more quickly inland but more slowly offshore, highlighting the contrasting dynamics across the region.
- Land–sea breeze circulations and coastal winds exert a variable influence on the spatial patterns and propagation of convection, modulated by ambient moisture availability and background wind strength.

The distinct diurnal patterns of clouds and rainfall identified in this study under different background wind regimes have important implications for the understanding environmental conditions associated with coral bleaching across the GBR. Previous studies have demonstrated strong links between cloud cover, surface radiative fluxes, SST variability, and coral bleaching. Within this broader context, our results show that propagation of cloud systems vary substantially between wind regimes, implying that the atmospheric conditions influencing reef environments can differ markedly depending on the prevailing large-scale circulation. In particular, the extensive late afternoon offshore propagation of convective cloud systems under north-westerly regimes suggests greater potential for cloud cover to extend over offshore reef areas, whereas the predominantly inland propagation observed under north-easterly and south-easterly regimes may reduce the influence of coastal convection on reef cloudiness. Because cloud cover is known to influence the radiative environment experienced by coral reefs, these contrasting cloud regimes may contribute to differences in environmental conditions conducive to bleaching.

While our study does not directly quantify radiative fluxes, ocean heat budgets, or bleaching impacts, these processes are likely modulated by the observed wind regimes and atmospheric structure, and may further influence SST variability. Given the limited observational evidence available, we cannot draw definitive conclusions regarding the local-scale mechanisms controlling convection initiation and propagation. Future research could employ high-resolution numerical modelling to better resolve and understand these processes. Additionally, deploying surface flux measuring instruments over the coastal ocean during the CBS would provide valuable constraints on air-sea interactions and could be integrated with high-resolution coupled atmosphere-ocean models to study the surface energy budget of the GBR during the CBS. Despite these limitations, our findings highlight the importance of incorporating diurnally evolving mesoscale weather processes, especially those linked to background wind regimes and coastal convection, into assessments and forecasts of coral bleaching risk during the austral warm season.

Code and data availability. The code for this project is hosted on GitHub: alanah-chapman. Data from the Level 1 Himawari–8 dataset (Lopez-Bravo et al., 2021a) is available at NCI. The Level 2 Australian Operational Weather Radar dataset (Soderholm et al., 2022) is available at NCI. BARRA–R2 regional reanalysis data (Su et al., 2022) is found on NCI Gadi.

Appendix A

A1

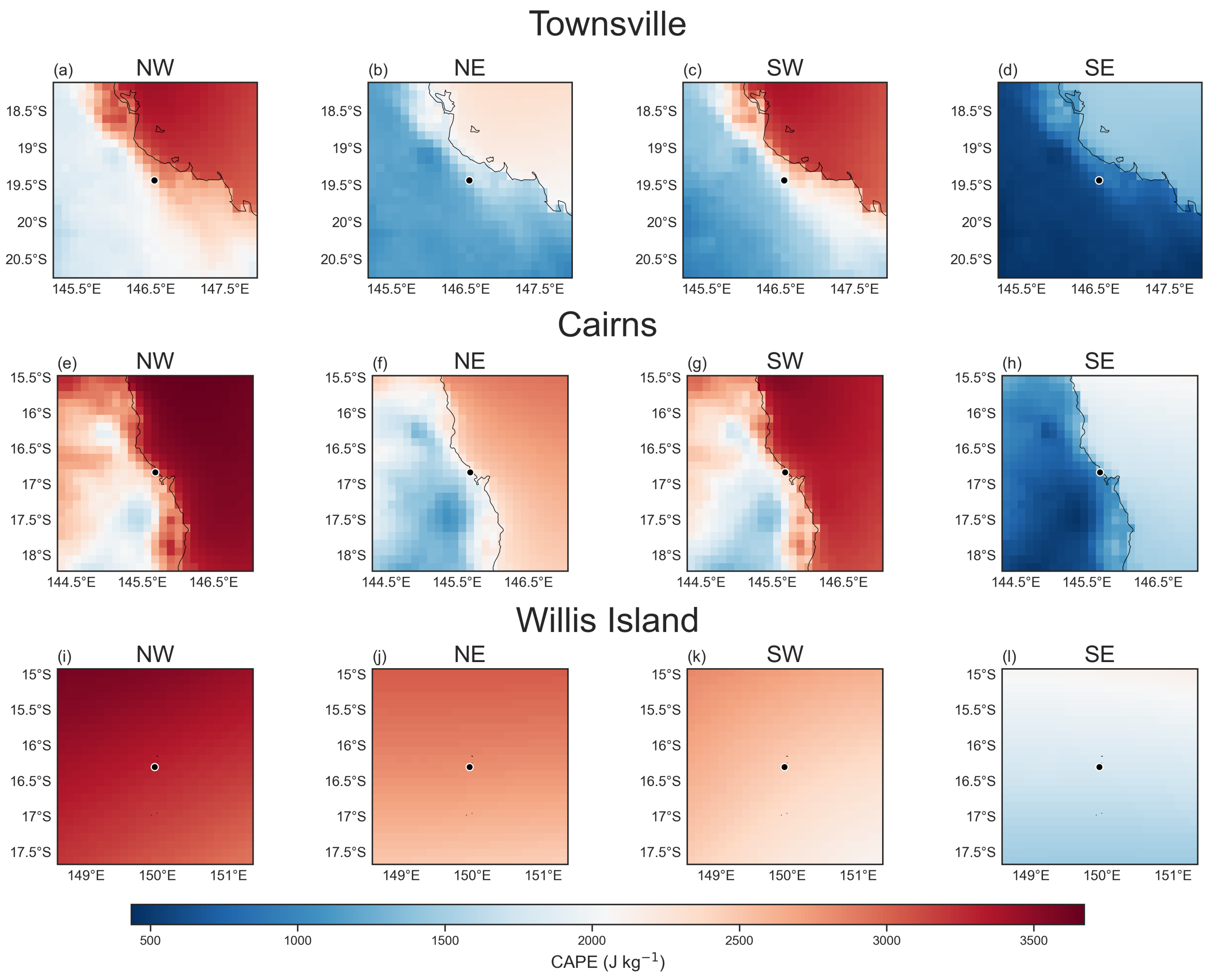

Figure A1. Townsville (a, b, c, d), Cairns (e, f, g, h) and Willis Island (i, j, k, l) BARRA-R2 Convective Available Potential Energy (J kg^{-1}) under each wind regime during the CBS between 1979 and 2025. Black markers indicates the radar locations for each site.

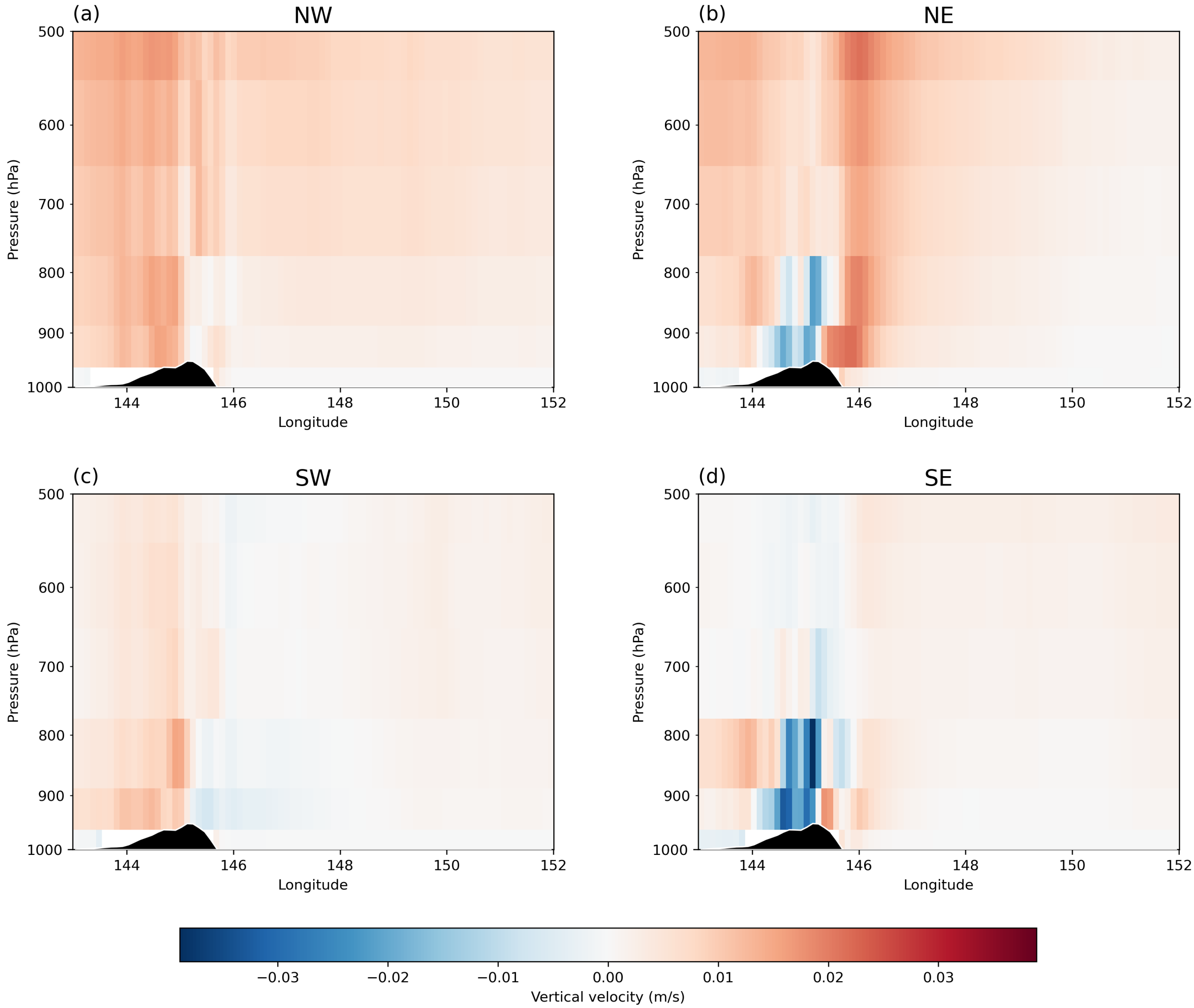

Figure A2. Vertical velocity (m s^{-1}) over the Hovmöller transect shown in Fig. 1. For each wind regime, the CBS mean (between years 1979–2025) is computed across the small latitude band. Mean topography from BARRA-R2 (16.6°S–17°S) is shaded in black, with elevation converted to pressure coordinates assuming a standard atmosphere.

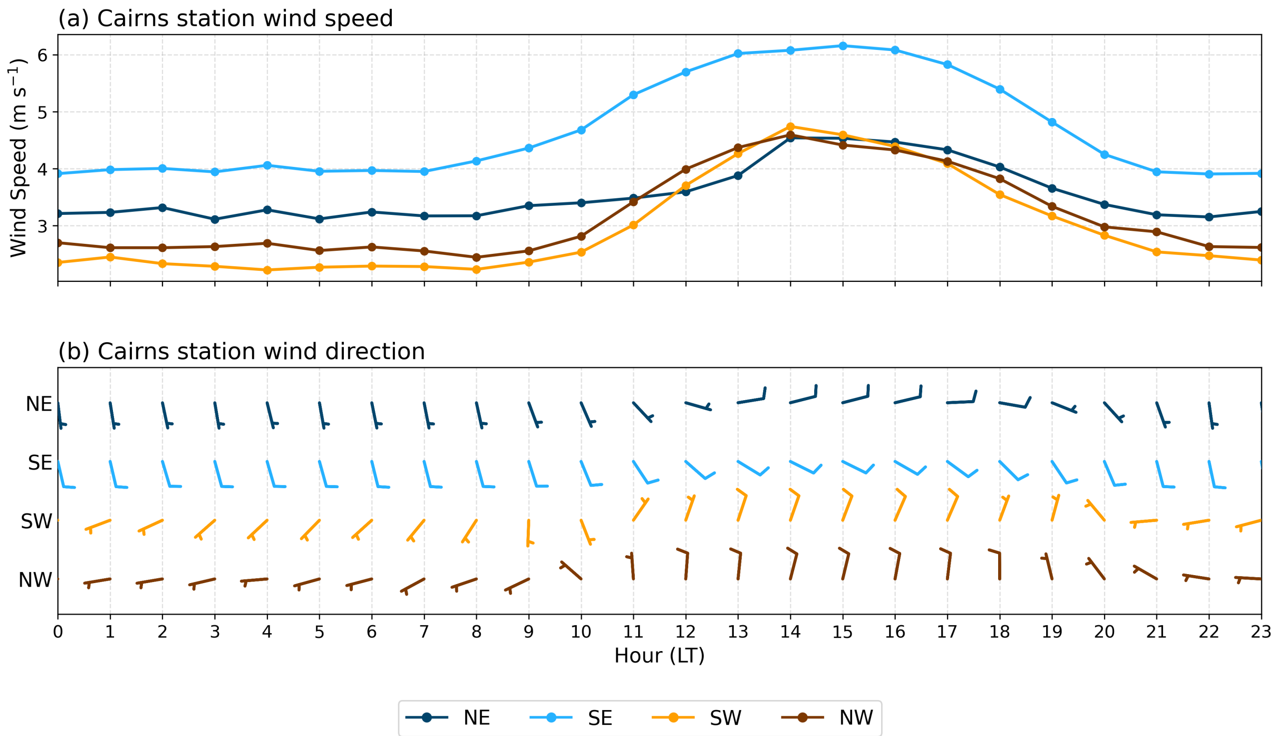

Figure A3. (a) Cairns station surface wind speeds and (b) wind direction (wind barbs) over the full CBS under each wind regime for the period 1990–2020.

Table A1. Coefficients used for the Z-R relation for each radar site (Pudashine et al., 2026). *Note the Z-R fit for Cairns was also used for Willis Island (which lacks rain gauges for calibration).

Site	a	b
Townsville	125	1.3
Cairns	85	1.35
*Willis Island	85	1.35

Table A2. Statistics on the 850 hPa winds averaged across each radar domain site for the four wind regimes. Note that sample sizes (N) shows the percentage of time periods under each regime for each site. These values were calculated for the CBS from BARRA–R2 wind fields between 1979–2023.

	Mean ($m\ s^{-1}$)	Median ($m\ s^{-1}$)	Maximum ($m\ s^{-1}$)	Minimum ($m\ s^{-1}$)	Standard Deviation ($m\ s^{-1}$)	N (%)
NE Regimes						
Townsville	6.29	5.91	38.21	0.04	3.28	23.43
Cairns	5.25	4.76	20.60	0.07	3.00	15.25
Willis Island	5.65	5.24	34.94	0.02	3.07	19.13
SE Regimes						
Townsville	7.95	7.85	40.05	0.08	3.21	62.54
Cairns	8.23	8.21	27.89	0.05	3.59	67.01
Willis Island	7.40	7.27	30.99	0.09	3.17	57.36
SW Regimes						
Townsville	4.35	3.86	22.21	0.07	2.75	7.49
Cairns	4.32	3.83	18.82	0.04	2.60	9.34
Willis Island	5.18	4.44	30.92	0.01	3.54	10.22
NW Regimes						
Townsville	4.63	3.83	21.57	0.03	3.23	6.19
Cairns	6.03	5.27	26.65	0.06	3.76	8.06
Willis Island	6.20	5.08	25.92	0.01	4.31	12.94

Author contributions. AC performed data analyses and contributed to writing the manuscript. YH contributed to project conception, results interpretation, and manuscript writing. CV contributed to results interpretation and research direction.

Competing interests. The authors declare that they have no conflict of interest.

Acknowledgements. The authors would like to acknowledge the Traditional Owners of the Great Barrier Reef and north-east Queensland. This research was undertaken with the assistance of resources from the National Computational Infrastructure (NCI Australia), an NCRIS enabled capability supported by the Australian Government.

Financial support.

This research is supported by the ARC Centre of Excellence for Climate Extremes (grant no. CE170100023) and the ARC Centre of Excellence for the Weather of the 21st Century (grant no. CE230100012). Yi Huang and Claire Vincent are further supported by an Australian Research Council Discovery Grant (grant no. DP230100639).

References

Aoki, S. and Shige, S.: Control of Low-Level Wind on the Diurnal Cycle of Tropical Coastal Precipitation, 37, 229–247, https://doi.org/10.1175/JCLI-D-23-0180.1, 2024.

As-syakur, A. R., Imaoka, K., Ogawara, K., Yamanaka, M. D., Tanaka, T., Kashino, Y., Nuarsa, I. W., and Osawa, T.: Analysis of Spatial and Seasonal Differences in the Diurnal Rainfall Cycle over Sumatera Revealed by 17-Year TRMM 3B42 Dataset, SOLA, 15, 216–221, https://doi.org/10.2151/sola.2019-039, 2019.

Berry, G. J. and Reeder, M. J.: The Dynamics of Australian Monsoon Bursts, Journal of the Atmospheric Sciences, 73, 55 – 69, https://doi.org/10.1175/JAS-D-15-0071.1, 2016.

Birch, C. E., Webster, S., Peatman, S. C., Parker, D. J., Matthews, A. J., Li, Y., and Hassim, M. E. E.: Scale Interactions between the MJO and the Western Maritime Continent, Journal of Climate, 29, 2471–2492, https://doi.org/10.1175/JCLI-D-15-0557.1, 2016.

Bowden, A. J., Jakob, C., and Soderholm, J.: Identification of Rainfall Events and Heavy Rainfall Events From Radar Measurements in Southeastern Australia, Journal of Geophysical Research: Atmospheres, 129, e2023JD039 253, https://doi.org/10.1029/2023JD039253, 2024.

Bui, H. X., Maloney, E. D., Short, E., and Riley Dellaripa, E. M.: Diurnal Cycle of Wind Speed and Precipitation Over the Northern Australia Coastal Region: CYGNSS Observations, Geophysical Research Letters, 50, e2023GL103 005, https://doi.org/https://doi.org/10.1029/2023GL103005, e2023GL103005 2023GL103005, 2023.

Christopoulos, C. and Schneider, T.: Assessing Biases and Climate Implications of the Diurnal Precipitation Cycle in Climate Models, Geophysical Research Letters, 48, e2021GL093 017, https://doi.org/https://doi.org/10.1029/2021GL093017, e2021GL093017 2021GL093017, 2021.

Clark, P., Roberts, N., Lean, H., Ballard, S. P., and Charlton-Perez, C.: Convection-permitting models: a step-change in rainfall forecasting, Meteorological Applications, 23, 165–181, https://doi.org/https://doi.org/10.1002/met.1538, 2016.

Covey, C., Gleckler, P. J., Doutriaux, C., Williams, D. N., Dai, A., Fasullo, J., Trenberth, K., and Berg, A.: Metrics for the Diurnal Cycle of Precipitation: Toward Routine Benchmarks for Climate Models, Journal of Climate, 29, 4461 – 4471, https://doi.org/10.1175/JCLI-D-15-0664.1, 2016.

Dao, T. L., Vincent, C. L., and Lane, T. P.: Multiscale Influences on Rainfall in Northeast Australia, 36, 5989–6006, https://doi.org/10.1175/JCLI-D-22-0835.1, publisher: American Meteorological Society Section: Journal of Climate, 2023.

Dao, T. L., Vincent, C. L., Huang, Y., Peatman, S. C., Soderholm, J. S., Birch, C. E., and Roberts, D. S.: Joint modulation of coastal rainfall in Northeast Australia by local and large-scale forcings, Quarterly Journal of the Royal Meteorological Society, 152, e70 027, https://doi.org/https://doi.org/10.1002/qj.70027, 2025a.

Dao, T. L., Vincent, C. L., Huang, Y., and Soderholm, J. S.: Modulations of local rainfall in northeast Australia associated with the Madden–Julian oscillation during austral summer, Quarterly Journal of the Royal Meteorological Society, 151, e4995, https://doi.org/https://doi.org/10.1002/qj.4995, 2025b.

Dipankar, A., Webster, S., Huang, X.-Y., and Doan, V. Q.: Understanding Biases in Simulating the Diurnal Cycle of Convection over the Western Coast of Sumatra: Comparison with Pre-YMC Observation Campaign, Monthly Weather Review, 147, 1615 – 1631, https://doi.org/10.1175/MWR-D-18-0432.1, 2019.

Hassim, M. E. E., Lane, T. P., and Grabowski, W. W.: The diurnal cycle of rainfall over New Guinea in convection-permitting WRF simulations, Atmospheric Chemistry and Physics, 16, 161–175, https://doi.org/10.5194/acp-16-161-2016, 2016.

Hohenegger, C., Brockhaus, P., and Schär, C.: Towards climate simulations at cloud-resolving scales, Meteorologische Zeitschrift, 17, 383–394, https://doi.org/10.1127/0941-2948/2008/0303, 2008.

Huang, Y., Lane, T., Ayat, H., Su, C.-H., Wales, S., Roberts, D., Petrelli, P., Vincent, C., Franklin, C., Dao, T. L., Chambers, C., Lopez-Bravo, C., Brown, A., Liu, S., Reid, K., Shaddock, R., Dix, M., Arblaster, J., and Jakob, C.: AUS2200: a high-resolution limited-area modelling project for Australia, Journal of Southern Hemisphere Earth Systems Science, 76, ES25 068, https://doi.org/10.1071/ES25068, 2026.

Huang, Z., Feng, M., Dalton, S. J., and Carroll, A. G.: Marine heatwaves in the Great Barrier Reef and Coral Sea: their mechanisms and impacts on shallow and mesophotic coral ecosystems, Science of The Total Environment, 908, 168 063, https://doi.org/10.1016/j.scitotenv.2023.168063, 2024.

Kendon, E. J., Stratton, R. A., Tucker, S., et al.: Enhanced future changes in wet and dry extremes over Africa at convection-permitting scale, Nature Communications, 10, 1794, https://doi.org/10.1038/s41467-019-09776-9, 2019.

Kong, Q. and Zhao, S.: Heavy rainfall caused by interactions between monsoon depression and middle-latitude systems in Australia: a case study, Meteorology and Atmospheric Physics, 106, 205–226, https://doi.org/10.1007/s00703-010-0060-5, 2010.

Lawrey, E. P. and Stewart, M.: Complete Great Barrier Reef (GBR) reef and island feature boundaries including Torres Strait (NESP TWQ 3.13, AIMS, TSRA, GBRMPA), https://doi.org/10.26274/vhj5-gr60, 2016.

Leahy, S. M., Kingsford, M. J., and Steinberg, C. R.: Do Clouds Save the Great Barrier Reef? Satellite Imagery Elucidates the Cloud-SST Relationship at the Local Scale, 8, e70 400, https://doi.org/10.1371/journal.pone.0070400, 2013.

Lopez-Bravo, C., Vincent, C. L., and Huang, Y.: Himawari-8 GeoCat 1.0.3 Australian Domain Level 2 v1.0, https://geonetwork.nci.org.au/geonetwork/srv/eng/catalog.search#/metadata/f7783_3730_7872_1101, 2021a.

Lopez-Bravo, C., Vincent, C. L., and Huang, Y.: Himawari-8 GeoCat 1.0.3 Australian Domain Level 1 v1.0, https://geonetwork.nci.org.au/geonetwork/srv/eng/catalog.search#/metadata/f7882_5837_8565_1103, 2021b.

Lopez-Bravo, C., Vincent, C. L., Huang, Y., and Lane, T. P.: A Case Study of a West Sumatra Squall Line Using Satellite Observations, Monthly Weather Review, 151, 523–543, https://doi.org/10.1175/MWR-D-21-0194.1, 2023a.

Lopez-Bravo, C., Vincent, C. L., Huang, Y., and Lane, T. P.: The Diurnal Cycle of Rainfall and Deep Convective Clouds Around Sumatra and the Associated MJO-Induced Variability During Austral Summer in Himawari-8, Journal of Geophysical Research: Atmospheres, 128, e2023JD039 132, https://doi.org/10.1029/2023JD039132, 2023b.

Lopez-Bravo, C., Vincent, C. L., Huang, Y., and Lane, T. P.: Impacts of the Madden-Julian Oscillation on Widespread Heavy Rainfall Over the Western Region of the Maritime Continent: Sumatra, Journal of Geophysical Research: Atmospheres, 130, e2025JD043 493, https://doi.org/https://doi.org/10.1029/2025JD043493, e2025JD043493 2025JD043493, 2025.

Love, B. S., Matthews, A. J., and Lister, G. M. S.: The diurnal cycle of precipitation over the Maritime Continent in a high-resolution atmospheric model: Diurnal Cycle Over the Maritime Continent, Quarterly Journal of the Royal Meteorological Society, 137, 934–947, https://doi.org/10.1002/qj.809, 2011.

Mapes, B. E., Warner, T. T., and Xu, M.: Diurnal Patterns of Rainfall in Northwestern South America. Part III: Diurnal Gravity Waves and Nocturnal Convection Offshore, Monthly Weather Review, 131, 830–844, https://doi.org/10.1175/1520-0493(2003)131<0830:DPORIN>2.0.CO;2, 2003.

Masson, S., Terray, P., Madec, G., Luo, J.-J., Yamagata, T., and Takahashi, K.: Impact of intra-daily SST variability on ENSO characteristics in a coupled model, 39, 681–707, https://doi.org/10.1007/s00382-011-1247-2, 2012.

May, P. T., Long, C. N., and Protat, A.: The Diurnal Cycle of the Boundary Layer, Convection, Clouds, and Surface Radiation in a Coastal Monsoon Environment (Darwin, Australia), Journal of Climate, 25, 5309–5326, https://doi.org/10.1175/JCLI-D-11-00538.1, 2012.

May, P. T., Trewin, B., Nairn, J. R., Ostendorf, B., Su, C.-H., and Moise, A.: Diurnal and Seasonal Variability of Near-Surface Temperature and Humidity in the Maritime Continent, 61, 1819–1834, https://doi.org/10.1175/JAMC-D-22-0032.1, 2022.

McGowan, H. and Theobald, A.: Atypical weather patterns cause coral bleaching on the Great Barrier Reef, Australia during the 2021–2022 La Niña, Scientific Reports, 13, 6397, https://doi.org/10.1038/s41598-023-33613-1, 2023.

McGowan, H., Sturman, A. P., MacKellar, M. C., Wiebe, A. H., and Neil, D. T.: Measurements of the local energy balance over a coral reef flat, Heron Island, southern Great Barrier Reef, Australia, Journal of Geophysical Research: Atmospheres, 115, https://doi.org/10.1029/2010JD014218, 2010.

Mori, S., Jun-Ichi, H., Tauhid, Y. I., Yamanaka, M. D., Okamoto, N., Murata, F., Sakurai, N., Hashiguchi, H., and Sribimawati, T.: Diurnal Land–Sea Rainfall Peak Migration over Sumatera Island, Indonesian Maritime Continent, Observed by TRMM Satellite and Intensive Rawinsonde Soundings, Monthly Weather Review, 132, 2021–2039, https://doi.org/10.1175/1520-0493(2004)132<2021:DLRPMO>2.0.CO;2, 2004.

Neale, R. and Slingo, J.: The Maritime Continent and Its Role in the Global Climate: A GCM Study, Journal of Climate, 16, 834–848, https://doi.org/10.1175/1520-0442(2003)016<0834:TMCAIR>2.0.CO;2, 2003.

NOAA National Geophysical Data Center: 2-minute Gridded Global Relief Data (ETOPO2) v2, https://doi.org/10.7289/V5J1012Q, 2006.

Pearson, K. J., Lister, G. M. S., Birch, C. E., Allan, R. P., Hogan, R. J., and Woolnough, S. J.: Modelling the diurnal cycle of tropical convection across the 'grey zone', Quarterly Journal of the Royal Meteorological Society, 140, 491–499, https://doi.org/https://doi.org/10.1002/qj.2145, 2014.

Peatman, S. C., Schwendike, J., Birch, C. E., Marsham, J. H., Matthews, A. J., and Yang, G.-Y.: A Local-to-Large Scale View of Maritime Continent Rainfall: Control by ENSO, MJO, and Equatorial Waves, Journal of Climate, 34, 8933 – 8953, https://doi.org/10.1175/JCLI-D-21-0263.1, 2021.

Peatman, S. C., Birch, C. E., Schwendike, J., Marsham, J. H., Dearden, C., Webster, S., Neely, R. R., and Matthews, A. J.: The Role of Density Currents and Gravity Waves in the Offshore Propagation of Convection over Sumatra, Monthly Weather Review, 151, 1757–1777, https://doi.org/10.1175/MWR-D-22-0322.1, 2023.

Pereira, L. G. and Rutledge, S. A.: Diurnal Cycle of Shallow and Deep Convection for a Tropical Land and an Ocean Environment and Its Relationship to Synoptic Wind Regimes, Monthly Weather Review, 134, 2688 – 2701, https://doi.org/10.1175/MWR3181.1, 2006.

Pudashine, J., Soderholm, J., Louf, V., Curtis, M., and Velasco-Forero, C.: Estimating Rain Rate from the Bureau of Meteorology Operational Weather Radar Network, Journal of Southern Hemisphere Earth Systems Science, manuscript under review, 2026.

Rauniyar, S. P. and Walsh, K. J. E.: Scale Interaction of the Diurnal Cycle of Rainfall over the Maritime Continent and Australia: Influence of the MJO, Journal of Climate, 24, 325–348, https://doi.org/10.1175/2010JCLI3673.1, 2011.

Richards, L. S., Siems, S. T., Huang, Y., Zhao, W., Harrison, D. P., Manton, M. J., and Reeder, M. J.: The Meteorological Drivers of Mass Coral Bleaching on the Central Great Barrier Reef during the 2022 La Niña, Scientific Reports, 14, 23 867, https://doi.org/10.1038/s41598-024-74181-2, 2024.

Richards, L. S., Siems, S. T., Huang, Y., Harrison, D. P., and Zhao, W.: Trade wind regimes during the Great Barrier Reef coral bleaching season, https://doi.org/10.5194/wcd-7-109-2026, 2026.

Sakaeda, N., Kiladis, G., and Dias, J.: The Diurnal Cycle of Tropical Cloudiness and Rainfall Associated with the Madden–Julian Oscillation, Journal of Climate, 30, 3999–4020, https://doi.org/10.1175/JCLI-D-16-0788.1, 2017.

Short, E., Vincent, C. L., and Lane, T. P.: Diurnal Cycle of Surface Winds in the Maritime Continent Observed through Satellite Scatterometry, Monthly Weather Review, 147, 2023 – 2044, https://doi.org/10.1175/MWR-D-18-0433.1, 2019.

Slingo, P. Inness, R. Neale, S. Woolnough, and G. Yang: Scale interactions on diurnal toseasonal timescales and their relevanceto model systematic errors, 46, https://doi.org/10.4401/ag-3383, 2003.

Soderholm, J., Louf, V., Brook, J., Protat, A., and Warren, R.: Australian Operational Weather Radar Level 2 Dataset, https://geonetwork.nci.org.au/geonetwork/srv/eng/catalog.search#/metadata/f8188_7912_6774_5057, 2022.

Stevens, B., Satoh, M., Auger, L., et al.: DYAMOND: the DYnamics of the Atmospheric general circulation Modeled on Non-hydrostatic Domains, Progress in Earth and Planetary Science, 6, 61, https://doi.org/10.1186/s40645-019-0304-z, 2019.

Su, C.-H., Dharssi, I., Le Marshall, J., Le, T., Rennie, S., Smith, A., Stassen, C., Steinle, P., Torrance, J., and Wang, C.: BARRA2: development of the next-generation Australian regional atmospheric reanalysis, 2022.

Tang, S., Gleckler, P., Xie, S., Lee, J., Ahn, M.-S., Covey, C., and Zhang, C.: Evaluating the Diurnal and Semidiurnal Cycle of Precipitation in CMIP6 Models Using Satellite- and Ground-Based Observations, Journal of Climate, 34, 3189 – 3210, https://doi.org/10.1175/JCLI-D-20-0639.1, 2021.

Vincent, C. L. and Huang, Y.: Meso- and microscale response to variation in cloudiness at three forested sites in the Maritime Continent, Quarterly Journal of the Royal Meteorological Society, 148, 418–433, https://doi.org/10.1002/qj.4212, 2022.

Vincent, C. L. and Lane, T. P.: Evolution of the Diurnal Precipitation Cycle with the Passage of a Madden–Julian Oscillation Event through the Maritime Continent, Monthly Weather Review, 144, https://doi.org/10.1175/MWR-D-15-0326.1, 2016.

Wheeler, M. C. and McBride, J. L.: Australasian Monsoon, in: Intraseasonal Variability in the Atmosphere-Ocean Climate System, pp. 147–197, Springer Berlin Heidelberg, ISBN 978-3-642-13914-7, https://doi.org/10.1007/978-3-642-13914-7_5, 2012.

Xie, S., Wang, Y.-C., Lin, W., Ma, H.-Y., Tang, Q., Tang, S., Zheng, X., Golaz, J.-C., Zhang, G. J., and Zhang, M.: Improved Diurnal Cycle of Precipitation in E3SM With a Revised Convective Triggering Function, Journal of Advances in Modeling Earth Systems, 11, 2290–2310, https://doi.org/https://doi.org/10.1029/2019MS001702, 2019.

Yamanaka, M. D., Ogino, S.-Y., Wu, P.-M., Jun-Ichi, H., Mori, S., Matsumoto, J., and Syamsudin, F.: Maritime continent coastlines controlling Earth's climate, Progress in Earth and Planetary Science, 5, 21, https://doi.org/10.1186/s40645-018-0174-9, 2018.

Yang and Slingo: The Diurnal Cycle in the Tropics, Monthly Weather Review, 129, 784–801, https://doi.org/10.1175/1520-0493(2001)129<0784:TDCITT>2.0.CO;2, 2001.

Yokoi, S., Mori, S., Katsumata, M., Geng, B., Yasunaga, K., Syamsudin, F., Nurhayati, and Yoneyama, K.: Diurnal Cycle of Precipitation Observed in the Western Coastal Area of Sumatra Island: Offshore Preconditioning by Gravity Waves, Monthly Weather Review, 145, 3745–3761, https://doi.org/10.1175/MWR-D-16-0468.1, 2017.

Zhao, W., Huang, Y., Siems, S., and Manton, M.: A characterization of clouds over the Great Barrier Reef and the role of local forcing, International Journal of Climatology, n/a, https://doi.org/10.1002/joc.7660, 2022.